POTENTIAL VORTICITY CONSERVATION IN UPPER TROPOSPHERIC FRONTS

by

LANCE F. BOSART
S.B., Massachusetts Institute of Technology
(1964)

SUBMITTED IN PARTIAL FULFILLMENT

OF THE REQUIREMENTS FOR THE

DEGREE OF

MASTER OF SCIENCE

at the

MASSACHUSETTS INSTITUTE OF TECHNOLOGY

July 1966

Signature of Author . . . . . .
Department of Meteorology, 18 July 1966

Certified by. . . . . .
Thesis Supervisor

Accepted by . . . . . .
Chairman, Departmental Committee on Graduate Students

POTENTIAL VORTICITY CONSERVATION IN UPPER TROPOSPHERIC FRONTS

by

LANCE F. BOSART

Submitted to the Department of Meteorology on 18 July 1966
in partial fulfillment of the requirements for the degree
of Master of Science

ABSTRACT

An intensifying upper tropospheric front is examined over the period 19 December 1963 at 1200 GMT to 20 December 1963 at 0000 GMT with particular regard to the validity of the conservation of the Ertel potential vorticity along trajectories ending in the baroclinic zone. The adiabatic assumption is justified by the extreme dryness of the frontal zone. A total energy equation is used as an aid in the trajectory construction.

With only one exception potential vorticity either increased or was conserved following the trajectories over the twelve hour period. These trajectories terminated in the central and western portions of the frontal zone as the eastern and probably most intense portion was over the Atlantic Ocean on 20 December 1963 at 0000 GMT. The potential vorticity increases were due to a large positive relative vorticity change on the northern periphery of the frontal zone and a marked stability increase on the southern periphery of the frontal zone. Diabatic effects could not explain the observed increases in potential vorticity. Rather turbulent processes in the atmosphere seem important. In particular, mesoscale motions may be exerting an influence on the synoptic features. Finally, an observation linking possible surface developments with the intensification of upper tropospheric baroclinic zones is presented.

Thesis Supervisor: Frederick Sanders
Title: Associate Professor

ACKNOWLEDGEMENT

Special thanks must go to several people whose aid made this thesis possible. My thanks go to Mrs. Jane McNabb for typing the paper and to Miss Isabelle Kole for drafting the more difficult accompanying figures and instructing me in the use of drafting equipment.

Thanks go to fellow students, Mike Wallace and Ken Campana, for occasional fruitful discussions. The help of Bill Sommers and Bob Ulchak with the more tedious aspects of the paper must not go unrecorded.

Of course, special thanks go to Professor Frederick Sanders without whose invaluable help and inspiration this thesis would not have been possible.

TABLE OF CONTENTS

I. INTRODUCTION

A. Historical Background

What is a front? The question is not asked to be facetious but to indicate the often widespread differences of opinion about them among meteorologists today. Surface fronts were first postulated by Bjerknes (1919) school just after the first world war to mark boundaries of air masses with different characteristics. Since then they have brought both joy and disillusionment to synoptic meteorologists searching for an infallible tool to forecast the weather. Yet, despite evidence to the contrary some meteorologists still insist that the observed weather changes can be explained by frontal movements. Even today, one often observes fronts moved about on surface maps like opposing armies in all the war games played in the various world capitals.

With the advent of good upper air coverage fronts have been found in the middle and upper troposphere. For better or worse we are stuck with the name "front". However, what one means here are baroclinic zones of varying intensity. These baroclinic zones are characterized by strong vertical wind shears through various stable layers. Other features of these baroclinic zones include an often large mixing ratio decrease in the vertical and high potential vorticity values. These baroclinic zones or fronts are not rare phenomena in the atmosphere but are almost independent of the more familiar surface front as Sanders (1954) and many others have shown. These upper level frontal zones usually first appear on the western sides of troughs and then intensity

as they descend around to the southeast side of the trough where they are strongest at 500 and 600 mb.

B. Recent Developments

Reed and Sanders (1953) and Sanders (1954) have found that these baroclinic zones are characterized by the largest subsidence at the warm edge of the frontal boundary. This resulted in an intensification of the horizontal temperature gradient. Reed (1955) in a case study found that the intense portion of the frontal zone consisted of a thin wedge of stratospheric air which had descended down to 700 and 800 mb. He considered that the frontal boundaries were a folded portion of the original tropopause. The circulation within the frontal zone was thermally indirect. Reed (1956) further noted that "surface cyclogenesis accompanied or slightly preceded the strengthening of the upper level front." Inspection of Reed's figures disclosed that the front was associated with the first upstream 500 mb vorticity maximum from the one associated with the strong surface cyclone. More will be said about this feature later.

The Ertel conservation of potential vorticity theorem following an air parcel along an isentropic surface has proved to be an invaluable aid for studying upper tropospheric fronts. Non conservation of this quantity will result if a vertical gradient of diabatic heating exists or if a component of the curl of the friction force exists normal to an isentropic surface. Staley (1960) has evaluated these two effects. His results show potential vorticity increases in the lower stratosphere

and upper troposphere on the cold side of the front. Negative potential vorticity changes occur within the frontal zone and around the entire periphery of the positive area. Staley finds that the potential vorticity changes are everywhere due to the vertical gradient of diabatic heating rather than the curl of the frictional force.

Additional support for the stratospheric origin of the high potential vorticity air within a frontal zone came from Reed and Danielsen (1959). Danielsen in a detailed study in 1960 showed that the original radiosonde traces contained many stable laminae which tended to persist in time. In addition, isentropic trajectories established a stratospheric source for many of these stable laminae. This tended to support the concept of a folded tropospause. Further support came in 1961 when Danielsen used a total energy relation as an aid in the construction isentropic trajectories.

Campana (1965) investigated an intense frontal zone through the use of isentropic trajectories involving satisfaction of the total energy equation and potential vorticity conservation. Like Reed, he found descent everywhere and evidence for an indirect thermal circulation. In addition, potential vorticity values increased along the higher isentropes through most of the frontal zone which Campana attributed to diabatic effects rather than frictional torques. This is in contrast to the potential vorticity decreases within the frontal zone found by Staley in 1960.

C. Goals of this Study

Many avenues for further study lie open. Among them are tropospheric stratospheric mass transport which has been studied by Danielsen, Staley and others and the problems of clear air turbulence for example. The main goal of this thesis will be to investigate the question of potential vorticity conservation during the formation of a strong upper tropospheric baroclinic zone. This issue is important because, for example, if potential vorticity increases with time in the frontal zone than the explanation of the folded tropopause with stratospheric air may not be entirely persuasive. In addition, it would be hoped that if non conservation is significant then some measure of diabatic or frictional effects might be attainable. In any event, it is hoped that this case study will add a further contribution to the record.

II. THEORETICAL BACKGROUND

A. Adiabatic Assumption

Let us now consider some of the fundamental theoretical background for this study. Most of the particulars have been elaborated by Campana (1965) and will not be considered here. Since proper trajectories are so critical to this study we will first examine some of the necessary constraints in this area. First of all, we will assume that the first law of thermodynamics for adiabatic flow may be written as:

$$\frac{d\theta}{dt} = 0 \qquad (1)$$

This states that potential temperature is conserved if one follows an air parcel. Of critical importance here is the adiabatic assumption. Any upward motion with subsequent condensation would ruin our efforts before we could start. Fortunately, the intensification of upper tropospheric fronts is generally associated with subsidence in relatively cloud free regions. Furthermore, the process takes place above the lower turbulent boundary layer and surface condensation effects.

B. Montgomery Stream Function

Since we will be working on surfaces of constant potential temperature the Montgomery stream function, Ψ , will prove invaluable for determining the geostrophic motion field. The Montgomery stream function

is defined as

$$\Psi = c_p T_\theta + g z_\theta \qquad (2)$$

where c_p is the specific heat of air at constant pressure, g is the acceleration of gravity, T_θ and z_θ are the temperature and height of the specific isentropic surface. Danielsen (1961) notes that if a reliable estimate of the geostrophic wind is to be made than Ψ must be measured to four significant figures. This would involve measuring T_θ to within $\pm$ 0.1°C which is not possible with present radiosonde equipment. Danielsen suggested as an alternate approach the use of Poisson's equation which relates T_θ to p_θ, the pressure on an isentropic surface. The latter leads directly to z_θ. In this manner the error in the computed Ψ up to the middle troposphere will be no worse than the error of the computed height of a constant pressure surface.

C. Total Energy Equation

In order to study potential vorticity changes during the intensification of the front isentropic trajectories will be needed. Initially, in constructing trajectories the best one can do is to make use of the ambiguous kinematic relation

$$D = \frac{V_1 + V_2}{2} \Delta t \qquad (3)$$

Here D is the total distance traversed by the parcel, V_1 is an

average geostrophic velocity for the first half time period, V_2 an average geostrophic velocity for the second half time period and Δt the total time period.

The essential roughness of (3) led Danielsen (1961) to develop a total energy equation as an aid in trajectory construction. This involves a deviation from the geostrophic path for a parcel. Such deviations will occur when the Ψ-field changes over a given time period such that the parcel is accelerated or decelerated. Now, in x, y, θ space the total derivative of Ψ may be written as

$$\frac{d\Psi}{dt} = \frac{\partial \Psi}{\partial t} + \bar{v} \cdot \nabla \Psi + \frac{d\theta}{dt} \frac{\partial \Psi}{\partial \theta} \qquad (4)$$

Under our assumption of adiabatic motion the last term in (4) is zero. The vector equation for horizontal frictionless motion on an isentropic surface may be expressed as:

$$\frac{d\bar{v}}{dt} = -\nabla \Psi - f(\hat{k} \times \bar{v}) \qquad (5)$$

where f is the Coriolis parameter and $\hat{k}$ is the unit vertical vector. Following Danielsen (1961) take the dot product of $\bar{v}$ with (5) and add dt to (4). The resulting equation is integrated over the length of the trajectory to yield:

$$\Psi_2 - \Psi_1 + \frac{V_2^2}{2} - \frac{V_1^2}{2} = \int_1^2 \frac{\partial \Psi}{\partial t} dt \qquad (6)$$

where the subscripts f and i refer to conditions at the final and initial times respectively. In this equation Ψ is a sum of the potential and internal energies while $\frac{V^2}{2}$ is a measure of the kinetic energy of the air parcel.

The right hand side of (6) can be approximated by a still to be specified time interval in Ψ at the initial, middle and final points of the trajectory. Graphical subtraction of the analyzed Ψ fields will do the trick in this case. Thus a practical form of Danielsen's total energy equation is:

$$\Psi_f - \Psi_i + \frac{V_f^2}{2} - \frac{V_i^2}{2} \approx \frac{\Delta\Psi_f + \Delta\Psi_i + 2\Delta\Psi_m}{4} \quad (7)$$

where the subscript m refers to the value at the mid point of the trajectory and Δ refers to a Ψ change over a fixed time period. Descent must take place along the trajectories for otherwise (7) would have to include a term involving the increase in Θ due to the release of latent heat. In addition, as Danielsen notes, care must be taken for parcels which originate on the anticyclonic side of the jet because more than one point may satisfy (3) and (7). This arises because the gradient of Ψ and V are negatively correlated.

D. Potential Vorticity

The crux of the trajectory analysis will depend upon the concept of conservation of potential vorticity. A theorem for this was first

established by Ertel in 1942. Rather than stating the theorem a proof based partly on physical reasoning will be included*. The fluid is assumed inviscid and a scalar quantity Θ is postulated such that Θ is a function of pressure, p, and density ρ, alone. This scalar quantity will satisfy (1). Consider a surface on which Θ is a constant. A curve C encloses an area A as shown in fig. 1

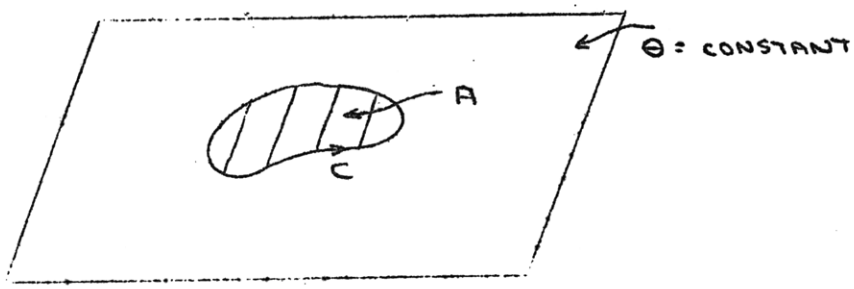

FIG. 1

The circulation, Γ, around this closed curve is defined by:

$$\Gamma = \oint_C \bar{u} \cdot d\bar{s} \qquad (8)$$

where $\bar{u}$ is the velocity vector. Now we may write

---

* Based in part on M.I.T. 18.61 course notes of Professor Joseph Pedlosky.

$$\frac{d\Gamma}{dt} = \frac{d}{dt}\oint \bar{u}\cdot d\bar{s} = \frac{d}{dt}\iint \nabla\times\bar{u}\cdot\bar{n}\, dA \qquad (9)$$

or

$$\frac{d\Gamma}{dt} = \frac{d}{dt}\iint \bar{\omega}\cdot\bar{n}\, dA \qquad (10)$$

Here $\bar{\omega} = \nabla\times\bar{u}$ is the relative vorticity and $\bar{n}$ is the unit normal.

Let us now examine Kelvin's theorem. Noting (8) we may write

$$\Gamma_{in} = \oint_c \bar{u}_{in}\cdot d\bar{s} = \oint \bar{u}\cdot d\bar{s} + \oint(\bar{\Omega}\times\bar{r})\cdot d\bar{s} \qquad (11)$$

where the subscript in refers to the inertial frame and the other symbols have their usual meanings in that case.

$$\therefore\ \Gamma_{in} = \oint \bar{u}\cdot d\bar{s} + \iint \bar{n}\cdot\left\{\nabla\times(\bar{\Omega}\times\bar{r})\right\} dA \qquad (12)$$

$$\therefore\ \Gamma_{in} = \oint \bar{u}\cdot d\bar{s} + \iint \bar{n}\cdot\left\{\bar{r}\cdot\nabla\bar{\Omega} - \bar{\Omega}\cdot\nabla\bar{r} + \bar{\Omega}(\nabla\cdot\bar{r}) - \bar{r}(\nabla\cdot\bar{\Omega})\right\} \qquad (13)$$

Thus,

$$\Gamma_{in} = \oint \bar{u}\cdot d\bar{s} + \iint 2\bar{\Omega}\cdot\bar{n}\, dA \qquad (14)$$

But,

$$\Gamma_{in} = \Gamma + \iint 2\bar{\Omega}\cdot\bar{n}\, dA \qquad (15)$$

Thus, ignoring friction,

$$\frac{d\Gamma}{dt} = -\frac{d}{dt}\iint 2\bar{\Omega}\cdot\bar{n}\,dA - \oint \frac{\nabla p}{\rho}\cdot ds \tag{16}$$

$$\therefore \frac{d\Gamma}{dt} = -\frac{d}{dt}\iint 2\bar{\Omega}\cdot\bar{n}\,dA + \iint \frac{\nabla\rho\times\nabla p}{\rho^2}\cdot\bar{n}\,dA \tag{17}$$

Noting (10) we are led to a statement of Kelvin's theorem:

$$\frac{d}{dt}\iint \bar{\omega}\cdot\bar{n}\,dA = -\frac{d}{dt}\iint 2\bar{\Omega}\cdot\bar{n}\,dA + \iint \frac{\nabla\rho\times\nabla p}{\rho^2}\cdot\bar{n}\,dA \tag{18}$$

Consider now a Γ which lies completely in a constant Θ surface and moves with the fluid. We know that along $\nabla\rho\times\nabla p$ both ρ and p are constant. Since $\Theta = \Theta(p,\rho)$ only $\nabla\rho\times\nabla p$ must lie in a constant Θ surface. Thus,

$$\iint \frac{\nabla\rho\times\nabla p}{\rho^2}\cdot\bar{n}\,dA \tag{19}$$

and (18) may be written as

$$\frac{d}{dt}\iint (\bar{\omega}+\bar{F})\cdot\bar{n}\,dA = 0 \tag{20}$$

where $\bar{F} = 2\bar{\Omega}$. Consider now two closely spaced constant surfaces as shown in fig. 2. The mass enclosed by the cylinder which is constant following the motion is given by

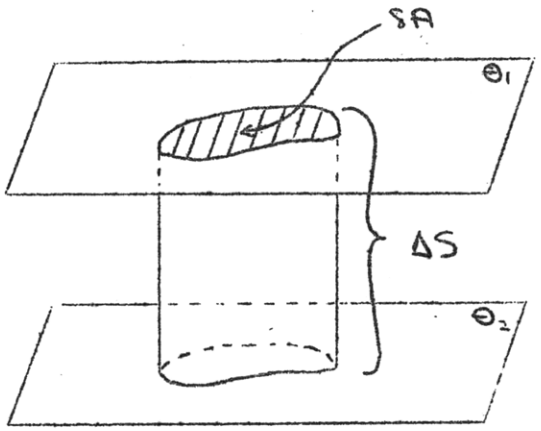

FIG. 2

$$m = \rho \delta A \Delta S \tag{21}$$

But,

$$\Delta\theta = \frac{\partial\theta}{\partial n}\Delta S \quad \text{or} \quad \frac{\partial\theta}{\partial n} = \frac{\Delta\theta}{\Delta S} \tag{22}$$

Thus,

$$\Delta S = \frac{\Delta\theta}{\partial\theta/\partial n} \quad \text{and} \quad \delta A = \frac{m}{\rho \Delta S} \tag{23}$$

Substituting into (20) we have:

$$\frac{\partial}{\partial t}\left[\left(\frac{\omega_n + f_n}{\rho}\right)\frac{\partial\theta}{\partial n}\,\frac{m}{\Delta\theta}\right] = 0 \tag{24}$$

where ω_n and f_n are parallel to $\hat{n}$. Since m and $\Delta\theta$ are constant we have

$$\frac{\partial}{\partial t}\left[\left(\frac{\omega_n + f_n}{\rho}\right)\frac{\partial\theta}{\partial n}\right] = 0 \tag{25}$$

of finally,

$$\frac{\partial}{\partial t}\left[\left(\frac{\vec{\omega}+\vec{f}}{\rho}\right)\cdot\nabla\theta\right]=0 \qquad (26)$$

Taking the component of absolute vorticity in the direction of the θ gradient and making use of the hydrostatic approximation with $\nabla\theta \approx \hat{k}\frac{\partial\theta}{\partial z}$ we may finally write:

$$\frac{\partial}{\partial t}\left\{-g\left[\zeta_\theta+f\right]\frac{\partial\theta}{\partial p}\right\}=0 \qquad (27)$$

Here ζ_θ is the relative vorticity on an isentropic surface and we ignore the difference between f and f_θ which is on the order of 10^{-6} sec^{-1}. If the frictionless and adiabatic assumptions are not made than a formal derivation (Campana 1965) yields the following results.

$$\frac{\partial}{\partial t}\left[-g\left(\zeta_\theta+f_\theta\right)\frac{\partial\theta}{\partial p}\right]=-g\left(\zeta_\theta+f_\theta\right)\frac{\partial}{\partial p}\left(\frac{\partial\theta}{\partial t}\right) \qquad (28)$$
$$-g\frac{\partial\theta}{\partial p}\mathcal{F}_n$$

where $\mathcal{F}_n$ is the component of the curl of the friction force in the direction of $\nabla\theta$ and the first term on the right takes into account that the vertical variation of heating is the largest contribution to diabatic effects.

If we consider (27) for the moment we see that $\frac{\partial\theta}{\partial p}$ represents the stability of an air parcel in up and down motion. This term is always negative. After some thought and experimentation it was decided

to evaluate this term by a centered finite difference approximation with a θ interval of eight degrees Kelvin such that

$$\frac{\partial \theta}{\partial p} \approx \frac{\theta_{i+8} - \theta_{i-8}}{\Delta p} \qquad (29)$$

Compana (1965) used a θ interval of four degrees Kelvin but it was felt that the eight degree interval was less sensitive to uncertainties of analysis and was still a good measure of the gross characteristics of the front. The relative vorticity, ζ_θ, on an isentropic surface is computed in the following manner.

$$\zeta_\theta = \frac{\partial v}{\partial r_\theta} + \frac{v}{r_\theta} \qquad (30)$$

where v is the wind speed and r_θ is the radius of curvature of the streamlines. A similar finite difference technique involving a horizontal increment of 120 nautical miles is used to evaluate the shear term, $\frac{\partial v}{\partial r_\theta}$. The units involved here are sec^{-1}. The curvature term is evaluated as $v \frac{\partial \phi}{\partial s_\theta}$ where s_θ is parallel to the streamline and ϕ is the wind direction in radians. With 120 nautical miles as the distance increment this term is again evaluated by finite difference techniques.

E. Factors which Influence Potential Vorticity

Since the upper level wind directions in data available on teletype

have been rounded off to 10 degrees errors are quite likely in $\bar{\gamma}_\theta$. The saving grace here is that wind directions in the area of interest are pretty much uniform. Because of the steeper slope of θ surfaces compared to isobaric surface the relative vorticity measured on the former is often anticyclonic and the latter cyclonic for the same area at the same time. Danielsen (1964) shows how when a front forms in the troposphere $\bar{\gamma}_p$ increases, the stability increases but $\bar{\gamma}_\theta$ decreases. Thus there must be a divergence of air on a constant θ surface for $\bar{\gamma}_\theta$ to decrease. Note that these changes are compatible with the conservation of potential vorticity.

The results of this study and many others generally established that the stability term was the most important in determining the size of P where P is defined as:

$$P \equiv -g\left(\bar{\gamma}_\theta + f\right)\frac{\partial\theta}{\partial p} \tag{31}$$

Simply on this basis we would expect to find P values in stratospheric air to exceed P values in tropospheric air by one or more orders of magnitude. Let us now examine what effects can lead to the non conservation of P. We have from (28)

$$F_n = \bar{n}\cdot\nabla\times\bar{\tau} \approx \left(\frac{\partial\tau_y}{\partial x} - \frac{\partial\tau_x}{\partial y}\right)_\theta \tag{32}$$

where $\bar{\tau}$ is the stress vector. Now, Staley (1960) has made some

rough estimates of both terms on the right hand side of (28). He found that the vertical variation of heating term was approximately 10^{-14} deg cm gm^{-1} while the normal component of the curl of the frictional force to the isentropic surface was approximately 10^{-15} to 10^{-16} deg cm gm^{-1}. It should be emphasized as Staley notes that these estimates may be off by several orders of magnitude. The effects of friction in the free atmosphere, radiational processes, eddy heat conduction and latent heat release are so poorly known as to make any estimates quite speculative. Yet later on we shall find it necessary to make some additional comments about these effects. Let us now turn to a consideration of the synoptic events for the case of December 1963.

III. SYNOPTIC SITUATION: 19-20 DECEMBER 1963

This particular case was chosen because it had one of the strongest 500 mb temperature gradients in Professor Sanders' survey of the 1963-64 season. The 500 mb maps for this period revealed the existence of a sharp temperature gradient from the Great Lakes eastward through New England on 20 December 1963 at 0000 GMT. The front was at its sharpest on 20 December at 0000 GMT in comparison to relatively weak frontal boundaries twelve hours earlier and later.

At 0000 GMT on 19 December 1963 the 500 mb map revealed a large ridge anchored over the Rocky mountains and a deepening trough centered over Virginia. A secondary vorticity maximum was centered just north of Lake Superior. The surface map at this time showed a weakening 989 mb storm centered near Syracuse and a deepening 1006 mb secondary forming southeast of Nantucket. An east-west dry cold front was located just north of Minnesota in connection with the upper air vorticity maximum there. By 19 December 1200 GMT the deepening secondary storm was down to 974 mb and was located 400 miles east of Boston. See fig. 3. The good cold advection into the trough aloft foretold of the deepening off the east coast as can be seen from fig. 4. By this time the 500 mb vortex was almost pin wheel shaped with the next upstream vorticity maximum centered near Sault Sainte Marie. The sharpening upper level front was associated with this latter vorticity maximum. Reference to the synoptic details at the time of fig. 3 reveals the complete absence

of precipitation with the surface cold front except for minor activity along the lee shores of the Great Lakes.

On the twentieth at 0000 GMT our now sharp upper level front is associated with a barely distinguishable cold front at the surface (see fig. 5) and a moderate vorticity maximum at 500 mb. Yet despite these innocuous features the temperature gradient has increased to nearly 20°C in almost 240 nautical miles (line AB in fig. 6). Meanwhile our surface storm has deepened to an almost fantastic 956 mb centered over northeastern Nova Scotia. The 500 mb trough in this region is difficult to discern because of the absence of data, not surprising in view of the hurricane force winds. Thus, at first glance the connection between the surface storm and the upper level front seems minimal. The partial low level cloudiness beneath the front seems to reflect daytime heating by the ice free and relatively warm Great Lakes of the bitter cold air mass rather than any extensive moisture associated with the upper level front.

IV. LOCATION OF THE FRONT

A. Collection of Pertinent Data

In order to locate the front the pertinent radiosonde data for the 19 December 0000 GMT through 20 December 1200 GMT was punched on cards to be run by the MIT meteorology department isentropic program. The number of individual radiosonde stations to run for each time period was determined on the basis of the area of significant vertical wind shear. A shear of twenty knots in 2000 feet was arbitrarily considered to be significant. This vertical shear was usually associated with a significant change in the vertical lapse rate and a rapid decrease in mixing ratio through the frontal zone. A fairly substantial ring of stations around the critical wind shear area was then chosen in order to assure data of enough horizontal extent for the trajectory analysis.

The computer program evaluated the pertinent data at each station for $\ominus$ surfaces at 4°K intervals ranging in general from 267°K to 327°K. All the essential information was to be found between these surfaces. For each station on every $\ominus$ surface the program computed the pressure in mb, mixing ratio in g/kg, relative humidity, wind direction to the nearest whole degree, wind speed in m sec^{-1}, Ψ in m^2 sec^{-2} and the total energy in m^2 sec^{-2}. Errors may result because significant temperature points on the sounding are left to the discretion of the radiosonde operator and teletype wind data are rounded

off to the nearest ten degrees. In particular, the height of the intersection of the measured lapse rate with a given $\ominus$ level may be in slight error. However, we note that we are dealing with a strong feature whose spacial and temporal variations occur over a large area such that minor little errors will be relatively insignificant. Of more concern will be the analysis problem in southern Canada due to the sparcity of data.

B. Display of Front on Potential Temperature Surfaces

The first order of business is to display the front on constant pressure surfaces. Since the front is most likely located between 300 and 700 mb bounds on the necessary $\ominus$ levels were determined from the highest and lowest potential temperatures at these pressure levels respectively. In order to visualize what is happening in the vertical on each $\ominus$ level the pressure and the difference in pressure between this surface and the one 4°C higher is plotted at each station. Now, on each $\ominus$ level the pressure is analyzed in 50 mb increments along with the help of the difference field of the lower level obtained by graphical subtraction. Once a map of the pressure on a $\ominus$ surface is obtained it is very easy to get a picture of the $\ominus$ field at a specific pressure level. In order to insure that the analysis is as good as possible we make use of the relation.

$$\frac{\partial \theta}{\partial x} = - \frac{\partial \theta}{\partial p} \left(\frac{\partial p}{\partial x} \right)_{\theta} \qquad (33)$$

Here $\left(\frac{\partial p}{\partial x}\right)_\theta$ is evaluated on an isentropic surface while $\frac{\partial \theta}{\partial x}$ is evaluated on an isobaric surface. The right hand side of (33) can be written in finite difference form as:

$$-\frac{\partial \theta}{\partial p}\left(\frac{\partial p}{\partial x}\right)_\theta = -\frac{\Delta\theta}{\Delta p}\left(\frac{\Delta p}{\Delta x}\right)_\theta \qquad (34)$$

$\Delta\theta$ is arbitrarily set equal to four degrees Kelvin and Δp determined from the plotted sounding. Equation (34) should be satisfied if the analysis is correct. Thus, information that we have in the vertical is used to more accurately locate the front in the horizontal. Using the actual temperature gradient in locating the front would only enable us to see a more or less uniform change in temperature between stations whereas by employing the isentropic analysis the stability values at the various stations have been used to obtain a better idea of the frontal intensity and its horizontal location. Compare figs. 3 and 8.

Figures 7 through 9 show the front at 400, 500 and 600 mb respectively on the 19 December 1963 at 1200 GMT. The frontal zone is weakly defined at all three levels with a maximum gradient of about 8°K in 40 nautical miles. The orientation of the frontal zone is pretty much parallel to the flow. The situation 12 hours later on 20 December 0000 GMT for levels 400 through 700 mb is shown by figs. 10 through 13. We do not see the marked strengthening of the front that Campana observed in his case. Yet overall the frontal zone sharpened up somewhat.

The strongest gradient on 20 December at 0000 GMT is 12°K over 60 nautical miles at 500 mb. Unfortunately, we are only looking at the upwird and a portion of the middle part frontal zone. The easternost part of the front extends out over the Atlantic south of Long Island. The data hints that the frontal zone may be even stronger here but the actual analysis is uncertain because the Nantucket radiosonde observation was not available on 20 December at 0000 GMT.

C. Cross Sections of Potential Temperature and Isotachs

Two cross sections of the $\ominus$ surfaces and the isotachs were constructed on 20 December at 0000 GMT. Lines AB and CD in fig. 14 show the extent of the cross sections. It was felt that the data was accurate enough to draw direct cross sections normal to the flow instead of restoring to the necessity of a cross section based on radiosonde locations only. The thermal wind equation was used as a check on the analysis. Figure 15 corresponds to line CD and is an attempt to depict the conditions in the vicinity of the entrance to the front. The familiar packing of the isentropes within the front zone and the steepening of the isentropes in the region of maximum vertical wind shear is quite evident. The shift of the front to higher $\ominus$ values with increasing altitude is noticeable also. The jet is located above the region of strongest horizontal temperature gradient in the vicinity of 500 mb. Furthermore, the strong cyclonic shear north of the jet coupled with the expected stability indicate a rapid increase in potential vorticity

values. Figure 16 corresponds to line AB in fig. 14. Line AB was not placed any closer to the coast because of the data uncertainty close to the ocean. There is very little difference in the isentrope packing and isotach pattern between the two cross sections. This indicates the relatively steady state situation at least over the western half of the front at that time.

V. DISCUSSION OF RESULTS

A. Trajectories and the Ψ Fields

The task of constructing trajectories was by far the most time consuming and tedious. In order to improve the accuracy of the trajectories all end points on 20 December 0000 GMT were chosen at regularly reporting radiosonde stations. Unfortunately, all observations at Nantucket and the upper winds at Flint were unavailable for this time period. The winds and Ψ values at these two stations were determined geostrophically with the aid of the surrounding analyses. A small connection factor based on the analysis was applied because the winds were generally subgeostrophic in the area of interest.

The Θ surfaces chosen for the trajectory analysis were 299, 291 and 283°K. These surfaces best represented the top, middle and lower part of the frontal zone as can be seen from figs. 15 and 16. In general, the frontal zone stretched from the Great Lakes to New England at the higher elevations and stretched southward through Illinois to Virginia at lower elevations. This area plus periphery boundary values dictated the choice of stations for the end points of the trajectories. Next, a very careful analysis of the Ψ field was made at each Θ level. In drawing the Ψ isopleths most attention was paid to the wind field. The generally uniform wind direction lent confidence to this decision. Values of Ψ were drawn for every 600 m^2 sec^{-2}. A geostrophic velocity based on contour intervals for this increment is included in Appendix I.

The values of Ψ selected for the contours were identical to the ones Compana used for consistency. At several stations, expecially on the Θ = 299°K surface it was impossible to draw for the wind field and satisfy the Ψ value at the same time. In these situations the contours were drawn so as to satisfy the wind field. At the same time since graphical subtraction of the Ψ fields was used to get the right hand side of (7), the computed energy values on the left hand side were modified by the appropriate Ψ field change in order to be consistent. The time period involved in all computations was twelve hours. Similarly, the appropriate isogon and isotach fields were constructed for each level. The spacing of the Ψ isopleths was used to get geostrophic wind values as an aid to drawing isotach contours between the reporting radiosonde stations. The isogon analysis was constructed over the Ψ field on a light table. Every effort was made to sort out the systematic errors.

The first trajectories were constructed to satisfy (3) and without reference to (7) or (27). The procedure involved here was to trace a path backwards parallel to the Ψ isopleths for the last six hour period. This point was transferred to the Ψ analysis twelve hours earlier and the trajectory continued parallel to the Ψ isopleths for the first six hour period. The results are shown in figs. 17 through 19. No attempt was made to smooth the trajectories.

The smoothness and steadiness of the wind field over the twelve hour period is evident from most of the trajectories. The trajectories

terminating at Great Lakes stations are open to doubt indicating large local changes of wind velocity. This is in the more intense area of the front and hints that trajectory corrections may have to be made in this area.

B. Satisfaction of the Total Energy Equation

Trajectories at the expected points of interest were then constructed so as to satisfy the energy equation (7). Figures 20 through 22 show these trajectories. The superscript $\in$ after each letter indicates that the trajectory satisfies (7). For reference the end point of the trajectories which satisfy (3) have been labeled with the appropriate letter. Note that the trajectories in figs. 20 - 22 also satisfy (3) based on average geostrophic winds over their length. These figures also reveal that the air on the southern periphery of the frontal zone was accelerating in view of the less cyclonically curved trajectories. On the $\ominus$ = 291°K and $\ominus$ = 299°K surfaces trajectories ending at stations 637, 645 and 747 which satisfy (3) and (7)differ considerably from the trajectories which only satisfy (3). Station 637 is at the extreme entrance to the frontal zone while stations 645 and 747 are located more or less in a region of weak $\ominus$ gradient (see fig. 11). These three trajectories at each level initiated in the light wind area of a cold vorticity maximum at 500 mb so it is not surprising that they are much more anticyclonic as they undergo acceleration.

C. Conservation of Potential Vorticity

Obviously, the next step was to calculate P values using (27) subject to (29) and (30). Figures 23 through 25 show the P values at the final points of the θ = 283, 291 and 299°K surfaces respectively. In addition, on the θ = 299°K surface (fig. 25) values of P were calculated over New England and New York State at a number of points between rawinsonde stations. This was done, as will be explained later, because of the suspected low P value at station 486. Similarly, figures 26 through 28 show P values at the initial points of the trajectories on 19 December at 1200 GMT. The superscripts again refer to the trajectories which satisfy both (3) and (7). In all cases P values are given in units of °K/mb cm/sec^3 $\times 10^{-3}$. In figs. 27 and 28 P values were calculated at extra points to give a better resolution of the field in the vicinity of the potential vorticity maximum. These extra points are labeled by an X with a numerical subscript. Trajectories are again constructed but this time so as to satisfy (27) subject to (29) and (30) while hopefully satisfying (3). These trajectories are shown by figs. 29 through 31. The superscript ν refers to the fact that they conserve potential vorticity. Again, for reference the initial points of the trajectories which satisfy (3) along and (3) and (7) together are included. Unfortunately, no trajectory satisfying (3) and (27) could be drawn for ACK (506) because the absence of data made it impossible to calculate the final P value there.

Examination of figs. 29 through 31 clearly show that several of the

trajectories which satisfy (27) et al cannot even approximately satisfy the displacement relation, (3). Overall, there seems to be a potential vorticity increase over the twelve-hour period. In particular, attention should be paid to the areas with P values in excess of 15 units since this represents a lower bound on air that may be of stratospheric origin. Now, let us examine what happens on each of the Θ surfaces before any attempt at an explanation of the behavior is made. Note appendices II through IV. The initial and final values of P as well as the factors $\frac{\partial \Theta}{\partial p}$ and $(\zeta_\theta + f)$ are presented for each type of trajectory for the more interesting stations at each Θ level. Also presented is the twelve hour pressure change which is a rough measure of the average vertical velocity. If there is adiabatic descent everywhere along the trajectory than the mixing ratio should be conserved following the parcel.

First, let us examine the Θ = 283°K surface (fig. 29). Clearly, trajectories I^v, K^v, N^v and O^v cannot satisfy (3). While L^v satisfies (3) the difference between the initial location of L versus L^v makes these trajectories questionable. Now, if I^v were to satisfy (3) by pulling it back to I or I^a than it would be necessary to postulate a potential vorticity decrease. A slight stability decrease along with a ζ_θ decrease accounts for the P decrease. Similarly, if K^v, N^v and O^v are to satisfy (3) then fig. 31 indicates that P must increase. Here the mechanism

seems to be a near doubling of the stability values over the twelve hour period without a commensurate decrease in $\mathcal{J}_\theta$. In fact, $\mathcal{J}_\theta$ decreases only slightly along K^ν and increases somewhat along O^ν and N^ν when these trajectories are corrected so as to satisfy (3). Any attempt to reduce the difference between L and L^ν by relocating the initial point nearer to L^2 will result in a P decrease through a large $\mathcal{J}_\theta$ decrease and a slight $\frac{\partial \theta}{\partial p}$ decrease.

On the θ = 291°K surface (fig. 30) it is immediately clear that I^ν, J^ν, K^ν, N^ν, O^ν, R^ν, and S^ν cannot satisfy (3) and conserve P at the same time. Growth of P must take place if (J^ν, K^ν, N^ν, O^ν, R^ν and S^ν) are to be drawn so as to satisfy (3). Similarly, a slight decrease in P will take place if I^ν is redrawn so as to satisfy (3). However, this latter change may be due to an inadequate isotach analysis. On the 20 December at 0000 GMT station 486 is just north of an isotach maximum while station 405 is just south of this maximum. With the isotach gradient as strong as it is the relatively large distance between the two stations is significant. From the geostrophic winds calculated from the Ψ field analysis it seems quite reasonable that a stronger wind maximum than analyzed lies between stations 486 and 405. This would cause the shear term in $\mathcal{J}_\theta$ to increase enough so as to raise the final P value at station 486 thereby bringing about conservation of this quantity. A point to be noted is that the horizontal increment of 120 nautical miles used in evaluating derivatives by finite difference methods may not be accurate for the

data resolution in the vicinity of isotach maxima whose true positions are somewhat dubious.

The P increases for trajectories ending at stations 520, 637, 645 and 747 (K,N,O,S) is predominately due to a large stability increase as can be seen from appendix II. At the same time, however, there are also varying small increases in γ_θ. On the whole these four trajectories end in the western part of the frontal zone and tend to be located on the southern periphery of the zone between 500 and 600 mb. For the trajectory ending at 734 (R) the P growth results from a large increase in γ_θ and a small increase in stability. Similarly for the trajectory ending at 518 (J) the P growth results more from a γ_θ increase than a stability increase. However, the difference is not as pronounced as for trajectory R. These latter two trajectories terminate on the northern periphery of the frontal zone between 400 and 500 mb.

On the θ = 299°K surface we again note that trajectories I^ν, O^ν, R^ν and N^ν are incapable of satisfying the displacement relation. Of these four trajectories only I^ν corrected so as to satisfy (3) would show a P decrease. Again, as in the case of the same trajectory on the θ = 291°K surface the result seems spurious. On the 20 December at 0000 GMT on the θ = 299°K station 486 has the highest wind speed at 58 m sec^{-1}. Again, the ψ field analysis supports an argument for a 65 to 70 m sec^{-1} wind maximum just south of station 486. This difference would be enough to

enable one to draw an I^v which satisfies (3) as well. However, there is no doubt that if N^v, O^v and R^v are drawn so as to satisfy (3) than a P increase must result. In the case of the N and O trajectories there seems to be a large and almost unreasonable horizontal difference between the initial points of O versus O^2 and N versus N^2. Yet, in both cases there is clear cut P growth. The difference is that N^2 and O^2 show the P growth as the result of a $\frac{\partial \theta}{\partial p}$ increase with only a very slight positive change in γ_θ while N and O show the P growth as the result of a γ_θ increase with only minor changes in $\frac{\partial \theta}{\partial p}$. If the trajectories which satisfy (7) and (3) are accepted (N^0, O^2) then we again have the suggestion of P growth on the southern periphery of the frontal zone due to a marked stability increase with only a very slight γ_θ increase. On the other hand the definite P growth found when R^v is drawn so as to satisfy (3) is mostly the result of a large and positive γ_θ increase. Stability changes are nil with R^2 in very good agreement with R. Thus, as on the 291°K surface there is the suggestion for P growth on the northern boundary of the frontal zone, due to an increase in γ_θ. It should be emphasized that these changes are along an isentropic surface and not along a horizontal surface. Not shown in the figures are the many trajectories which were drawn so as to conserve P and satisfy the energy equation at the same time. It was impossible for the same trajectories in figs. 29 through 31 to satisfy the

displacement relation (3) as well. To satisfy (3) it was necessary to postulate P growth.

D. Moisture Analysis

The next step is to stand back and take a good look at the entire analyses. First of all, after some thought it became clear that the mixing ratio data was generally unreliable, due to the large number of motorboating values in the very dry air within the frontal zone. In a few cases, however, we were able to obtain useful results. For example, on the Θ = 283°K surface a mixing ratio increase occurs along N, N°, L° and L° despite slight to moderate descent. Motorboating and saturation problems are not important here. On the Θ = 291°K surface it seems difficult not to postulate an increase despite descent along the N and S trajectories. A slight increase may also take place along the L trajectories. Similarly, on the Θ = 299°K surface there may be a slight increase with descent along the L trajectories. Widespread motorboating nin the other cases makes comparisons impossible. Thus, we have a good example of an area of neglect in meteorology. The conservative nature of the mixing ratio is a very valuable feature under conditions of adiabatic descent. Unfortunately, until just this last year the standard radiosonde instruments had a low relative humidity bias and were incapable of measuring humidities below -40°C. This bias has been eliminated by new carbon elements

on the radiosondes in use for the last year. A recent article by Masterson et al (1966) indicates that water vapor measurements by balloon-borne frost-point hygrometers have provided very accurate relative humidity measurements in the upper troposphere and lower stratosphere. In fact, a moist layer with maximum relative humidities close to 80% has been discovered below the tropical tropopause but above the cut off of the conventional Weather Bureau radiosondes. Mixing ratios of less than 0.005 gm kg^{-1} have been measured accurately. It is very important that accurate humidity measurements like these become routinely available. This would lend a great deal more confidence to trajectory analysis and would probably be useful to diffusion and turbulent mixing studies.

E. Factors Effecting Non-Conservation of Potential Vorticity

There is very little doubt that a definite increase in potential vorticity occurred with one exception throughout the frontal zone as it intensified over a twelve hour period. The most stringent requirement on the trajectories is the conservation of P because $\frac{\partial \theta}{\partial t}$, $\frac{\partial}{\partial p}\left(\frac{\partial \theta}{\partial t}\right)$ and F_n must be zero for this to hold whereas only $\frac{\partial \theta}{\partial t}$ and friction must be zero for the energy equation to be satisfied. Now, we can think of the non-conservation of P as the result of three effects. One, the normal component of the curl of the friction force, F_n, to the isentropic surface is not zero but the flow is adiabatic. The trajectories are correct but P is not conserved in this case. Two,

the flow is adiabatic on a given isentropic surface but diabatic motions exist on adjacent surfaces. In this case, even though the isentropic trajectory is valid, diabatic motions on adjacent surfaces yield P changes. Three, the flow is not adiabatic so that the trajectories are wrong and P will not be conserved. In addition, stability changes are going to be effected mostly by diabatic motions whereas relative vorticity changes will be influenced mainly by frictional effects.

The surprising feature of this case is the generally positive changes in the relative vorticity, ζ_θ, along the trajectories where P increases. As the front intensifies and the isentropes are squeezed together we would expect ζ_θ to decrease in order to conserve P. This only seems to happen in the middle of the frontal zone viewed from above. To the south large stability increases go along with slight ζ_θ increases while to the north minor stability changes go along with large ζ_θ increases. Since the initial points of the trajectories were located between radiosonde stations it was necessary to make a map of the stability on 19 December 1200 GMT in order to calculate P values. Many of the initial points were located just north of the U. S. border in the data sparse region of southern Canada. Now, errors in stability can have significant effects on P calculations. With this error source in mind the necessary soundings for the 19 December 1200 GMT were scrutinized to see if the stability field could be remapped so as to increase the stability north of the Great Lakes. This would lead to higher initial P values

and reduce the P growth. The data did not justify doing this, however.

Another question to consider is the possible role of diabatic effects. Values of $\frac{\partial P}{\partial t}$ (31) were calculated for various changes of P up to 20 units under the assumption that friction was unimportant. This corresponded to a cooling rate of 0.8°K per day per 100 meters and was well within Moeller's (1951) cooling rates above cloud tops of 2 to 5°C per day per thousand feet. Cloudiness beneath the intensifying upper front over the twelve hour period was sparse with one exception. On the 19 December 1200 GMT cloudiness and some light snow flurry activity over Michigan and the eastern Great Lakes area was associated with a weak low just northeast of Green Bay. Cloud bases were in the vicinity of 2000 feet. The cloud type was generally stratocumulus. Twelve hours later the weak surface system had all but disappeared leaving some lee shore cloudiness and snow flurries in the eastern Great Lakes region. It must be remembered that at that time of the year the Great Lakes were relatively warm and ice free. Hence, they were able to supply moisture to the lower levels of the overlying bitter cold air mass. This shows up in figs. 32 and 33 which are plots of the relative humidities on the Θ = 283°K surface. Note the 40% relative humidity at 637 in fig. 32 and the 49% value at 528 in fig. 33.

The stratocumulus clouds at best are probably a couple of thousand feet thick and extend up to around the 850 mb level. This is well

below the 500 to 600 mb position of the $\ominus$ = 283 °K surface over the Great Lakes for the twelve hour period. Thus, the influence of cloud tops for radiational cooling and the associated stability changes seems minimal. Now, Staley (1965) has shown that the distribution of mixing ratio through a baroclinic zone in the upper troposphere can have a marked effect on the radiational cooling rate. The inversion is maintained or strengthened somewhat for mixing ratios which decrease rapidly upward from the inversion base. Similarly, the inversion tends to be weakened if this condition is not met. We will now try to show that this latter condition may have played a role in our case. Examination of the Buffalo (528) sounding for 20 December at 0000 GMT reveals a fairly moist layer up to $\ominus$ = 297 °K with a relative humidity of about 50% at $\ominus$ = 283°. The mixing ratio falls off only ever so slightly upward through the inversion and wind shear layer. On 19 December at 1200 GMT at stations (637) and (734) there is a slight hint of the relatively moist layer extending up to and slightly beyond the $\ominus$ = 283°K surface. Unfortunately an incomplete sounding at (637) and temperatures in the region of interest at (734) colder than -40 °C make it impossible to be certain of the humidity structure. This area includes a large part of the region through which trajectories I and L pass on the $\ominus$ =283°K surface. Thus one can only speculate that the P decrease along I and possible decrease along L on this surface is due to a slight destabilization. Otherwise, diabatic effects seem unimportant in this study. Reference to Appendix II shows the decrease in stability along I, I^2, L and L^2 to be the chief

reason for the P decrease. Note that while L^v satisfies (3) and (27) the large horizontal difference between L^v and L (fig. 29) arouses suspicion in the trajectory.

The positive relative vorticity changes stood out the most on the northern fringe of the frontal zone. Overall, the behavior was to markedly increase the stability of the frontal zone along the southern boundary while still increasing the relative vorticity there. As the front intensifies and the stability increases we would expect the relative vorticity to decrease if P is conserved. This does not happen and we have seen that diabatic effects do not offer much of a clue to the non-conservation of P. Our case would be strengthened if data were available for the western Atlantic ocean. All evidence points to the strongest portion of the frontal zone being offshore on 20 December at 0000 GMT. Comparison of figures 23 and 26 shows that the area of maximum P values increased over the twelve hour period on the lower Θ surface. A similar comparison on the Θ = 281 and 299 surfaces is not possible because the maximum P region is somewhere southeast of Nantucket on 20 December at 0000 GMT. Thus, one can only speculate that a similar area increase would be found on these surfaces.

VI. CONCLUSIONS

A. Role of Turbulent Processes

Thus, we are forced to the conclusion that frictional effects through the catch all F_n term (32) played a significant role in our case. This has not been previously found to be true for these upper tropospheric baroclinic zones. The potential vorticity either increased or was conserved with one exception within the frontal zone. Staley's (1960) claim for a P decrease on the cold boundary of an upper tropospheric front was nowhere substantiated. In addition, his assertion of P growth due chiefly to diabatic effects is not valid in this case. In a way the results are quite disappointing. So very little is known about turbulent processes in the free atmosphere that very few quantitative statements can be made. It may be quite likely that mesoscale atmospheric motions are important enough to effect synoptic scale features in this case.

If turbulent processes are indeed playing a role here than we are left with three possibilities, all somewhat unappealing. One, turbulence be it mesoscale or synoptic scale is somehow strengthening the jet gradient over the twelve hour period. This can take place either if the jet intensifies or the gradient across the jet axis increases. The data only hints at either of these possibilities, however. It seems unlikely the friction thought of in its dissipative sense can accomplish the above. Two, turbulent processes somehow act to form and strengthen temperature inversions within the layer of

strong vertical wind shear. This is an area in which mesoscale atmospheric motions may be important. For example, mesoscale motions may be responsible for the bringing together of stable laminae of the type found by Danielsen (1960. Viewed on a synoptic scale this would have the effect of creating a temperature inversion or a noticeable discontinuity in the lapse rate where one did not exist before. Of course, the same result could be accomplished by synoptic scale vertical motions but that does not rule out the former possibility.

We know from observation that the various patterns in the atmosphere all have a certain degree of organization. Individual cumulus clouds, for example, tend to be arranged in rows and the many small cumuli of late morning are often a few larger clouds by late afternoon. The downdraft from a thunderstorm can result in a psuedo cold front several times the diameter of the individual cell. A cluster of storms may yield a psuedo cold front tens of miles long. This front then possesses many of the observed features of a true synoptic scale front. The point here is that misoscale effects can operate so as to produce a system visible on the synoptic scale. By analogy, mesoscale motions may be operating in a similar manner in upper tropospheric baroclinic zones, although on a scale of tens of miles to a synoptic scale of hundreds of miles. The very dryness of these baroclinic zones should not hinder the analogy since, for example, numerical models have been able to generate synoptic scale systems like squall lines from mesoscale effects without incorporating the release of latent heat. See Sasaki (1962), for example. The latter, while

important, has yet to be shown to be both a necessary and sufficient condition for squall line development

B. Reliability of Entire Analysis

The third possibility is the most unappealing of all. Namely, that the analysis contains enough errors to render the results meaningless. It is hoped that this did not happen here. Every effort was made to make the analysis consistent through numerous cross checks. In addition, the painstaking trajectory analysis gave the author a good idea of the sensitivity of the various factors. Djuric (1961) has shown that the greatest source of error to trajectory analysis is the sparcity of radiosonde data coupled with roundoff errors in wind direction and inaccuracies in the wind speed as the result of the length of the sampling period. Danielsen has also studied these latter effects. After working with the data the author agrees with the conclusions. Undoubtedly, the trajectories still contain some errors but it is felt that they are the best possible with the given data. In particular, the sparcity of data in southern Canada lends uncertainty to the field analysis there because of the marked cyclonic curvature of the isopleths. Thus, isotach and especially isogon analysis is uncertain there. The only significant contributions of the curvature term of the relative vorticity to P evaluation occurs in regions of pronounced ψ curvature. However, a little experimentation in changing the ψ field to get somewhat different trajectories failed to alter any of the results.

C. Problem of Clear Air Turbulence

Perhaps the results of this study will impart momentum to the developing studies of turbulent processes and in particular mesoscale motions. The problem of clear air turbulence (CAT) is likely involved here also. Evidence has been offered that occurrences of CAT have been associated with upper tropospheric baroclinic zones. In turn, the whole problem is connected with the dynamics of the jet stream. Also, topographic features at the surface may play a role. It may be that the Great Plains on the downstream side of the climatological North American ridge is a favorable location for the formation of these intense baroclinic zones. One cannot help but wonder if some connection exists between these zones and the dynamics of stratospheric warming phenomena with particular regard to CAT. Charney and Drazin (1961) among others have shown that the western North American mountain barrier and the associated climatological 500 mb ridge are able to act as a source for a perturbation from below to trigger baroclinic instability in the polar night vortex. This is by no means to suggest that upper tropospheric fronts are related to stratospheric warming phenomena but that a common factor may exist. For example, substantial vertical motions are involved in both cases.

D. Stratospheric Origin of Trajectories

A further thought is indicated at this point. It has been shown by Reed, Danielsen and others for the cases that they have studied that air contained in the baroclinic extrusion is really of stratospheric

origin. This forms the basis for the folded tropopause argument. The results of this study do not dispute this claim but they offer another possibility. Stratospheric air may still be present within the frontal zone but the P growth over the twelve hour period may indicate that such air does not reach as close to the surface as otherwise thought. The whole point here is that the folded tropopause with air of stratospheric origin may not provide the entire explanation of high potential vorticity values within the frontal zone.

E. Surface - Upper Troposphere Interaction

One observation in conclusion that may be of interest follows. The formation and intensification of the upper tropospheric baroclinic zone was associated with the next upstream 500 mb vorticity maximum from one associated with a very intense surface cyclone. The same phenomenon can be noted from Campana's (1965) case. A quick check offered similar evidence for Staley's case in 1960 and Reed's case in 1955. Finally, a further check through all of Professor Sanders' cases for the 1963-64 winter season established that the above were not isolated observations. The more intense fronts at 500 mb were often associated with the vorticity maximum in the axis of the trough. The deepening surface storm was associated with the immediate downstream 500 mb vorticity maximum or at least are areas of positive vorticity advection. This suggests that some form of surface-tropospheric interaction may be associated with the upper level baroclinic zones. In any event the presence of a deep 500 mb trough seems to be a necessary condition for the formation of these baroclinic zones. The observations are of enough interest to warrant further study.

Appendix I

The following table presents the values of a distance increment, 2Δ, for various latitudes. It is used if the contours of Ψ are analyzed at intervals of 600 $m^2 sec^{-2}$. The number (and fraction) of contour intervals contained in 2Δ is multiplied by 10 to give the geostrophic velocity in m sec^{-1}.

Latitude (degrees)	2Δ (degrees of latitude)
25	8.8
30	7.4
35	6.5
40	5.8
45	5.2
50	4.8
55	4.5
60	4.2
65	3.9

Appendix II

θ = 283°K

	P_i	P_f	S_i	S_f	η_i	η_f	Δp
I	23.7	18.6	.133	.125	1.82	1.52	-17
I^a	26.3	-	.133	-	2.01	-	-30
I^c	-	-	.094	-	-	-	-77
K	19.0	23.2	.102	.174	1.90	1.36	-48
K^a	21.1	-	.113	-	1.90	-	-18
K^c	-	-	.119	-		-	-16
L	27.8	15.7	.143	.099	1.98	1.62	+63
L^a	23.7	-	.119	-	2.03	-	-14
L^c	-	-	.105	-	-	-	-45
N	12.9	27.7	.083	.172	1.60	1.64	-85
N^a	12.6	-	.083	-	1.54	-	-80
N^c	-	-	.143	-	-	-	0
O	10.2	22.2	.072	.148	1.45	1.53	-120
O^a	9.6	-	.070	-	1.40	-	-117
O^c	-	-	.109	-	-	-	-52

Subscripts i and f refer to the initial and final values respectively

$S \equiv \frac{\partial \theta}{\partial p}$ in units of °K mb^{-1}

$\eta \equiv \eta_{\theta+f}$ in units of 10^{-4} sec^{-1}

$P \equiv$ potential vorticity in units of 10^{-4} °K/mb cm/sec^3

$\Delta p \equiv$ pressure change in mb, minus sign indicates descent

Appendix III

Θ = 291°K

	P_L	P_F	S_L	S_F	η_L	η_F	ΔP
I	30.9	26.0	.170	.154	1.86	1.72	-21
I^e	31.5	-	.162	-	1.98	-	-21
I^v	-	-	.167	-	-	-	+6
J	26.6	35.5	.168	.195	1.62	1.86	-8
J^e	26.6	-	.168	-	1.62	-	-13
J^v	-	-	.176	-	-	-	-17
K	18.2	27.8	.124	.222	1.49	1.28	-102
K^e	9.6	-	.128	-	.76	-	-41
K^v	-	-	.152	-	-	-	-91
N	14.2	28.4	.095	.170	1.53	1.70	-142
N^e	17.5	-	.107	-	1.68	-	-106
N^v	-	-	.150	-	-	-	-76
O	8.5	25.4	.080	.152	1.08	1.69	-193
O^e	11.6	-	.086	-	1.37	-	-125
O^v	-	-	.136	-	-	-	-105
R	10.6	20.8	.084	.116	1.28	1.83	-39
R^e	6.9	-	.079	-	1.15	-	-51
R^v	-	-	.114	-	-	-	-13
S	7.8	10.3	.076	.098	1.04	1.08	-102
S^e	7.2	-	.064	-	1.14	-	-77
S^v	-	-	.080	-	-	-	-92

Appendix IV

Θ = 299°K

	P_i	P_f	S_i	S_f	η_i	η_f	ΔP
I	31.5	32.4	.211	-235	2.49	1.41	-63
I^s	41.6	-	.200	-	2.12		-30
I^v	-	-	.208	-	-		+17
N	26.5	29.7	.152	.160	1.78	1.89	-156
N^s	21.8	-	.107	-	2.07	-	-143
N^v	-	-	.151	-	-	-	-150
O	18.3	24.9	.133	.128	1.40	1.99	-190
O^s	19.7	-	.096	-	2.09	-	-165
O^v	-	-	.133	-	-	-	-177
R	24.8	34.7	.178	.178	1.42	1.99	-43
R^s	22.2	-	.162	-	1.40	-	-48
R^v	-	-	.216	-	-	-	-9

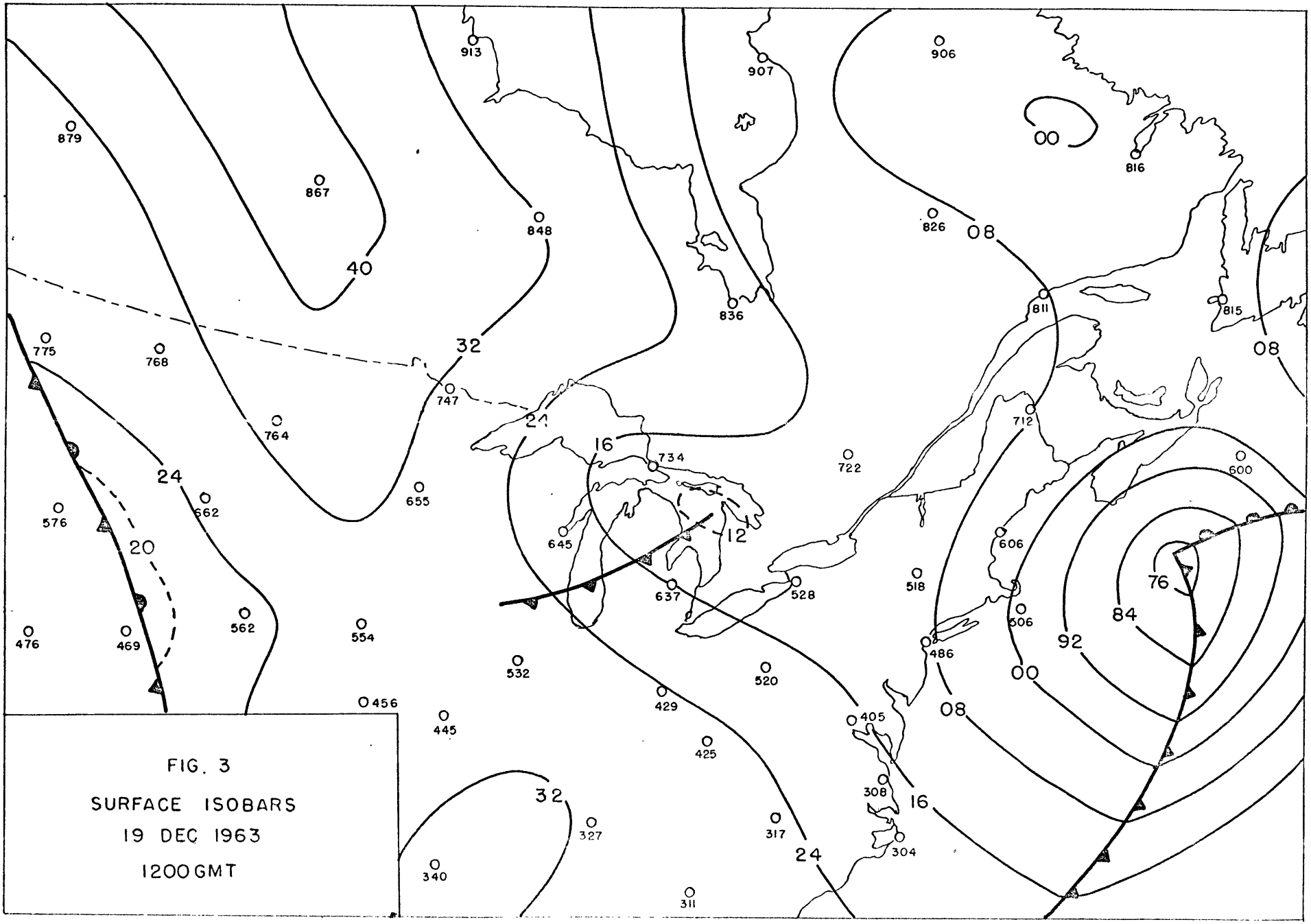

FIG. 3

SURFACE ISOBARS

19 DEC 1963

1200 GMT

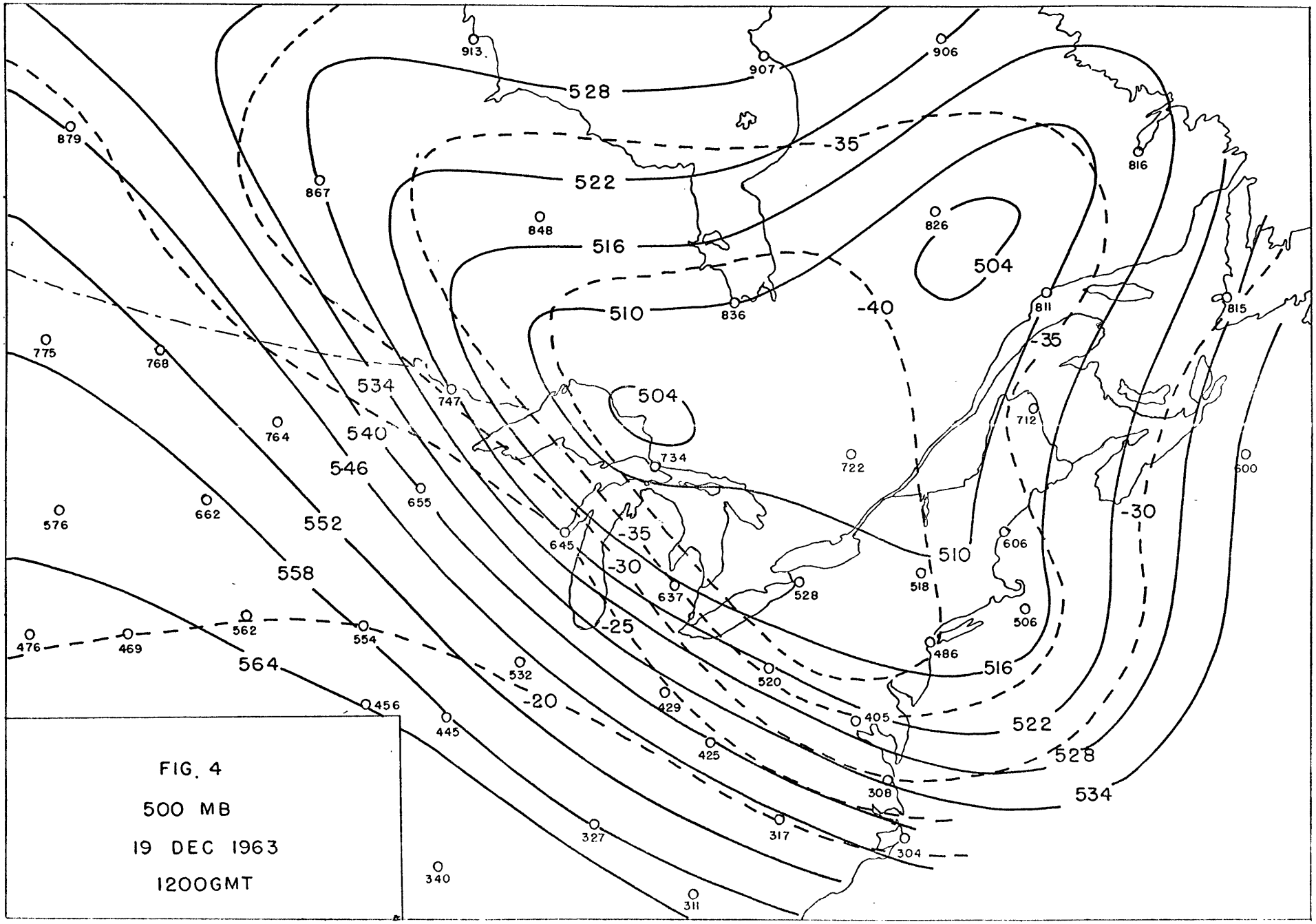

FIG. 4

500 MB

19 DEC 1963

1200GMT

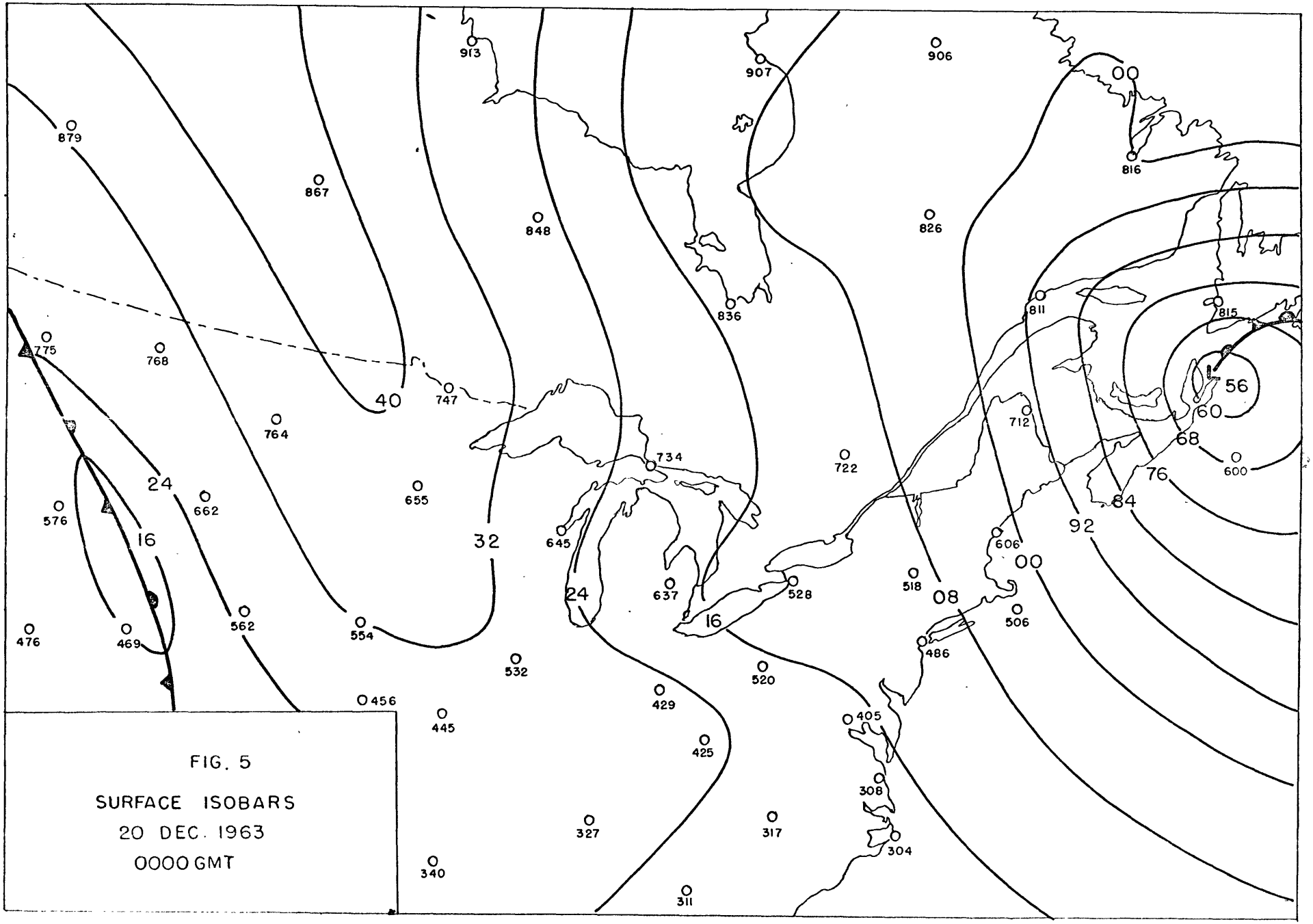

FIG. 5

SURFACE ISOBARS

20 DEC. 1963

0000 GMT

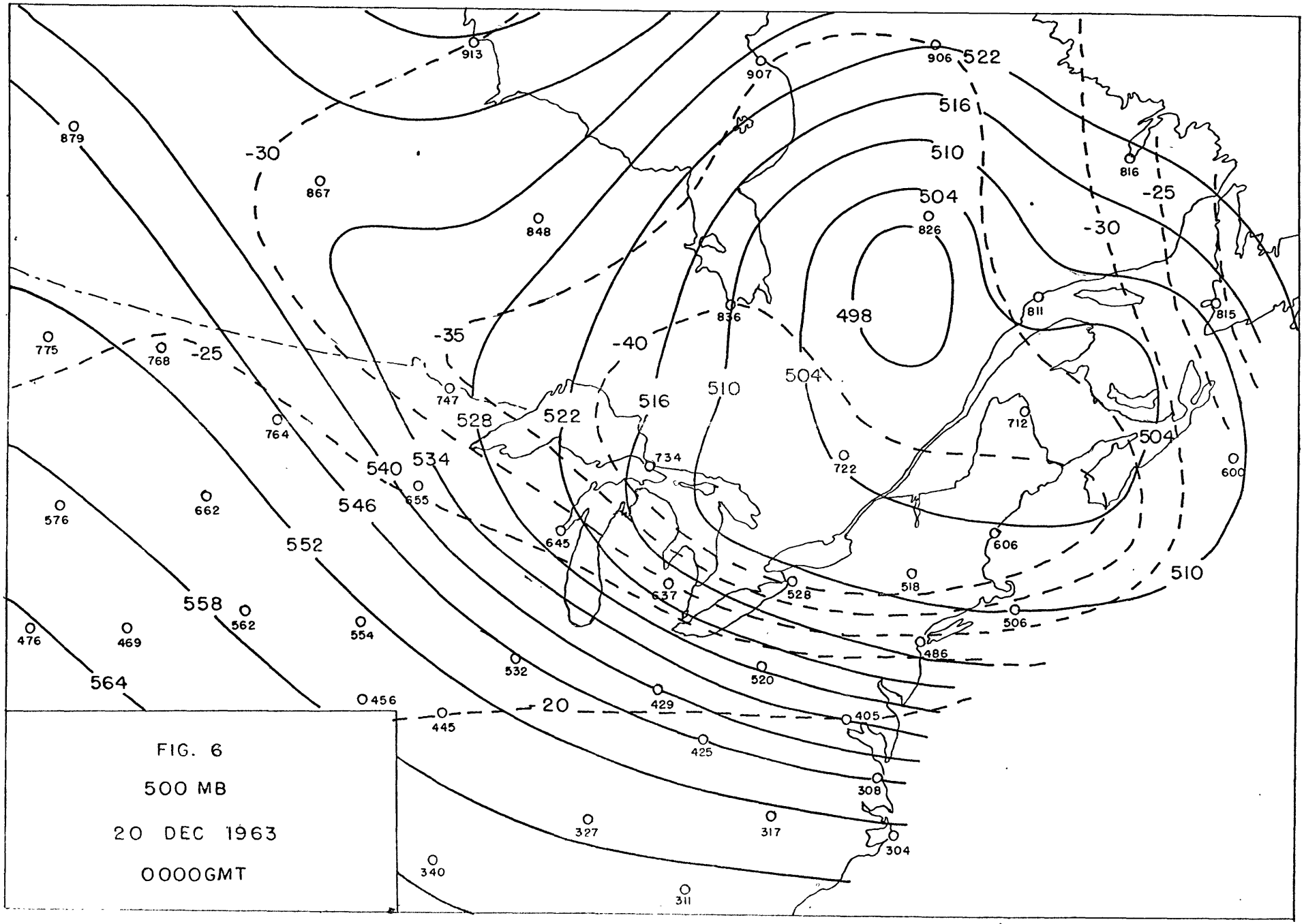
913
907
906
522
516
879
-30
510
816
867
504
-25
848
826
-30
498
836
811
815
775
768
-25
-35
-40
747
504
516
510
764
528
522
712
504
540
534
734
722
600
655
576
662
546
552
645
606
510
637
528
518
558
562
554
506
476
469
532
520
564
486
456
429
405
445
425
308
327
317
304
340
311
FIG. 6
500 MB
20 DEC 1963
0000GMT

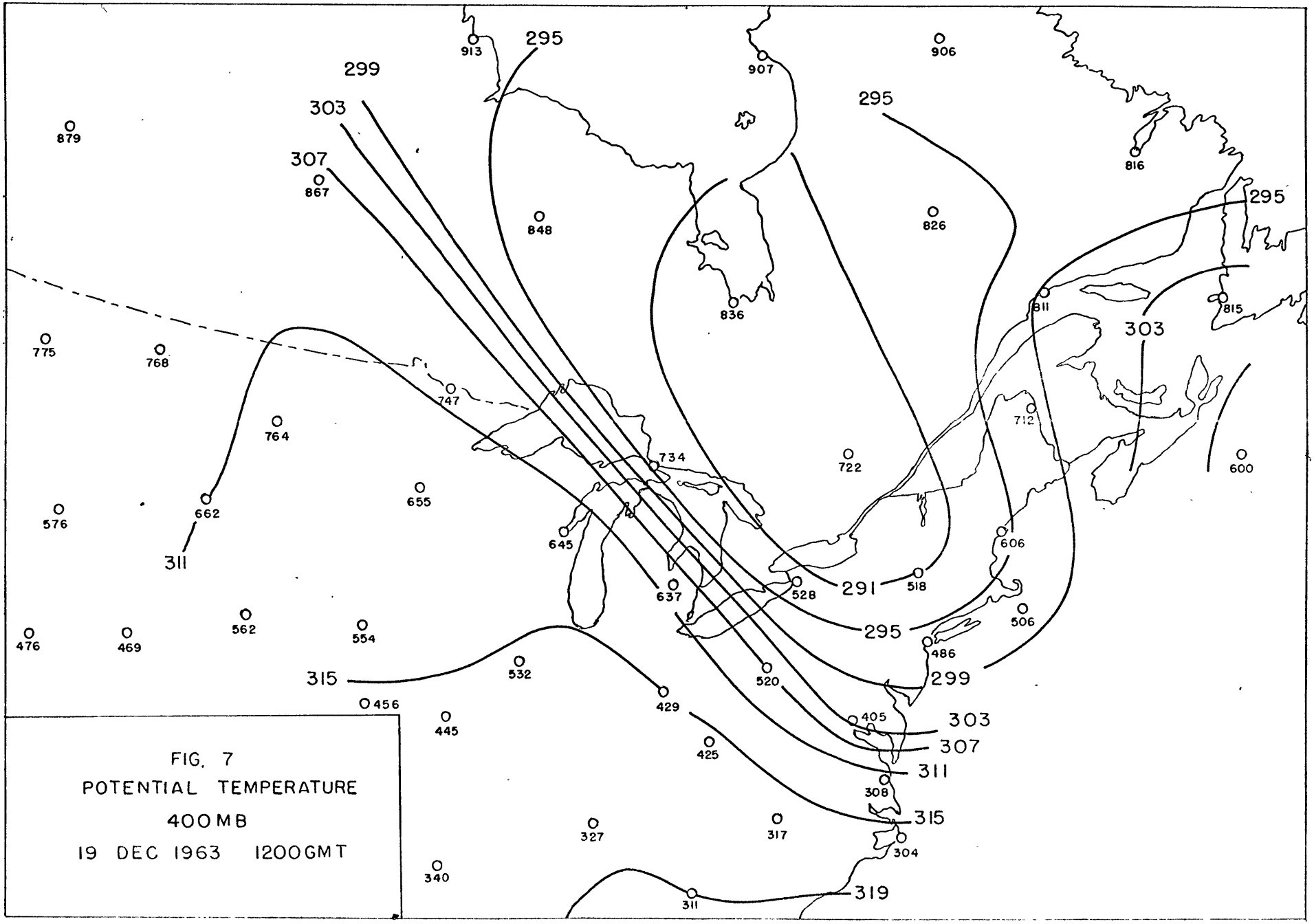

FIG. 7
POTENTIAL TEMPERATURE
400 MB
19 DEC 1963 1200 GMT

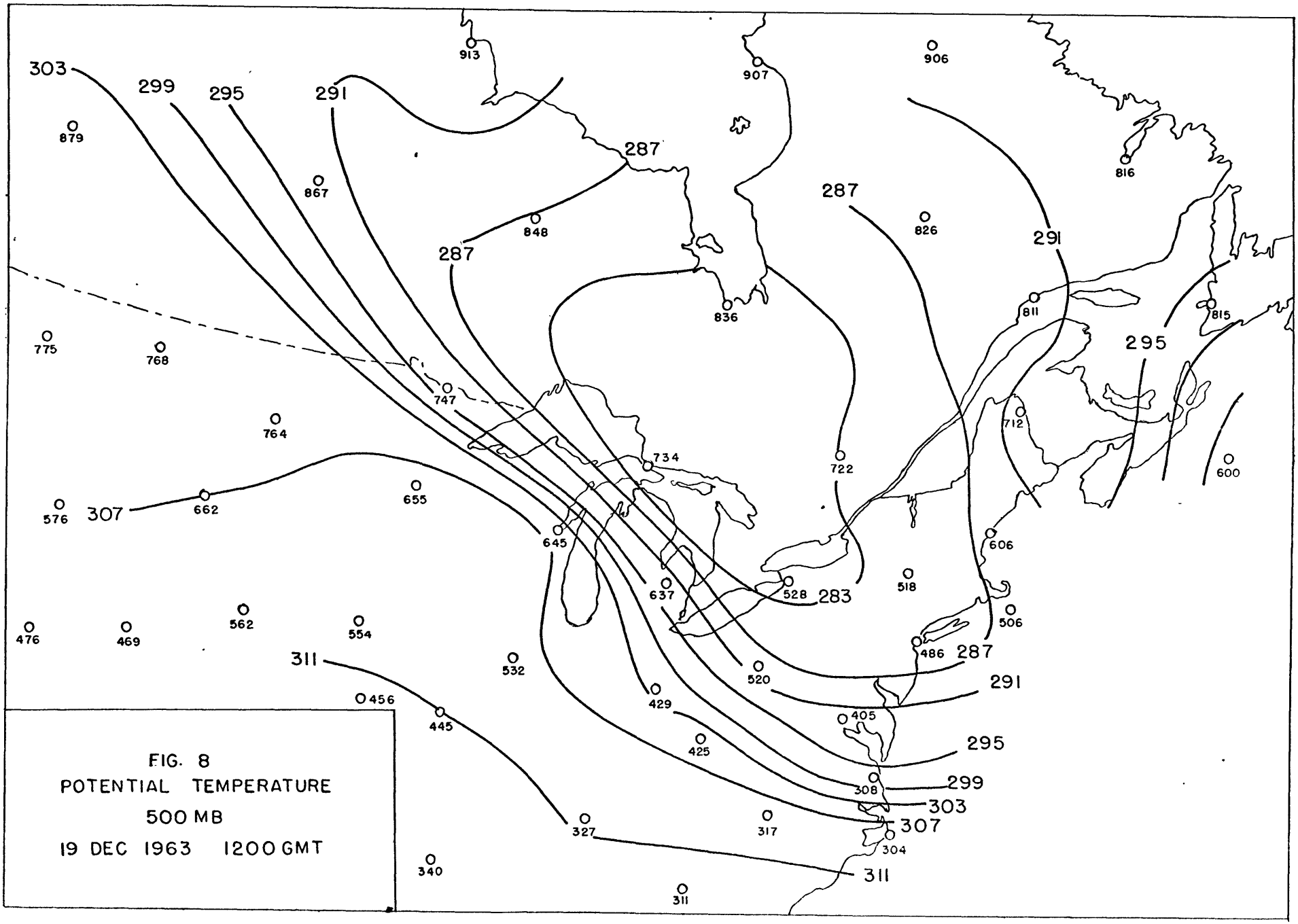
303
299
295
291
287
287
287
291
295
283
307
311
913
907
906
879
867
848
816
826
836
811
815
775
768
747
764
712
734
722
600
576
662
655
645
606
637
528
518
476
469
562
554
532
520
506
486
456
445
429
425
405
308
304
327
317
340
311
FIG. 8
POTENTIAL TEMPERATURE
500 MB
19 DEC 1963 1200 GMT

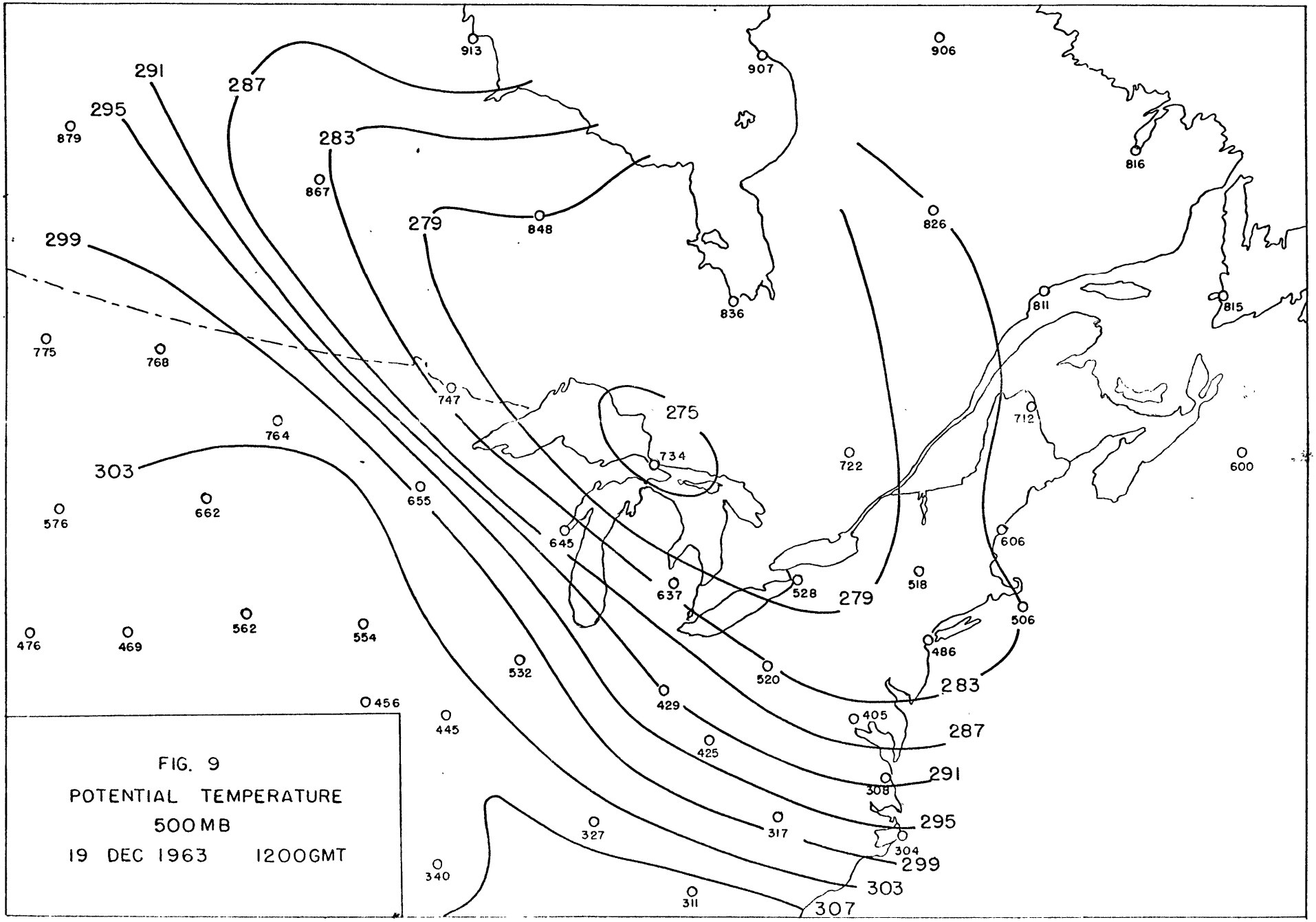

FIG. 9
POTENTIAL TEMPERATURE
500 MB
19 DEC 1963 1200GMT

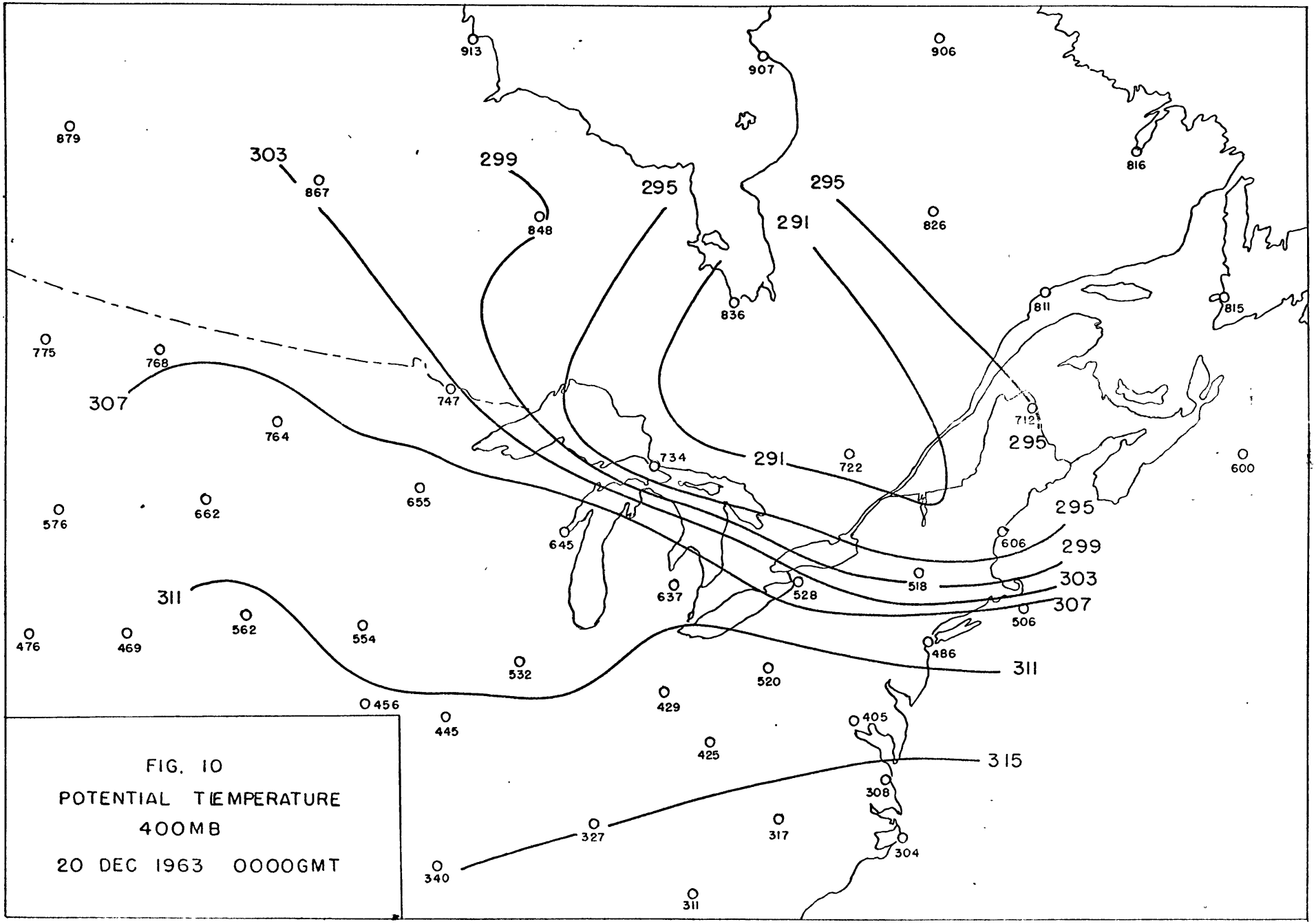

FIG. 10
POTENTIAL TEMPERATURE
400MB
20 DEC 1963 0000GMT

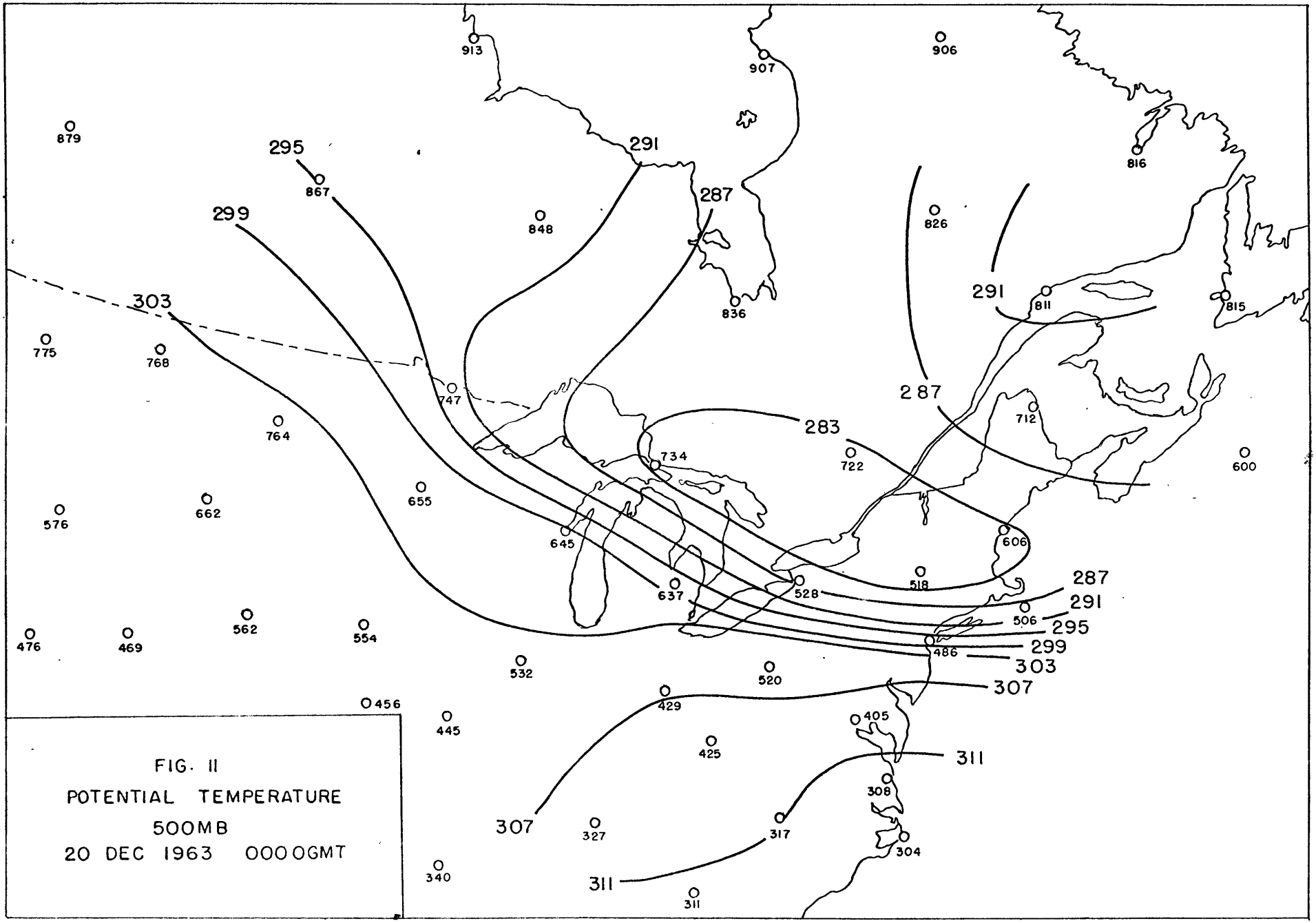

FIG. II
POTENTIAL TEMPERATURE
500MB
20 DEC 1963 0000GMT

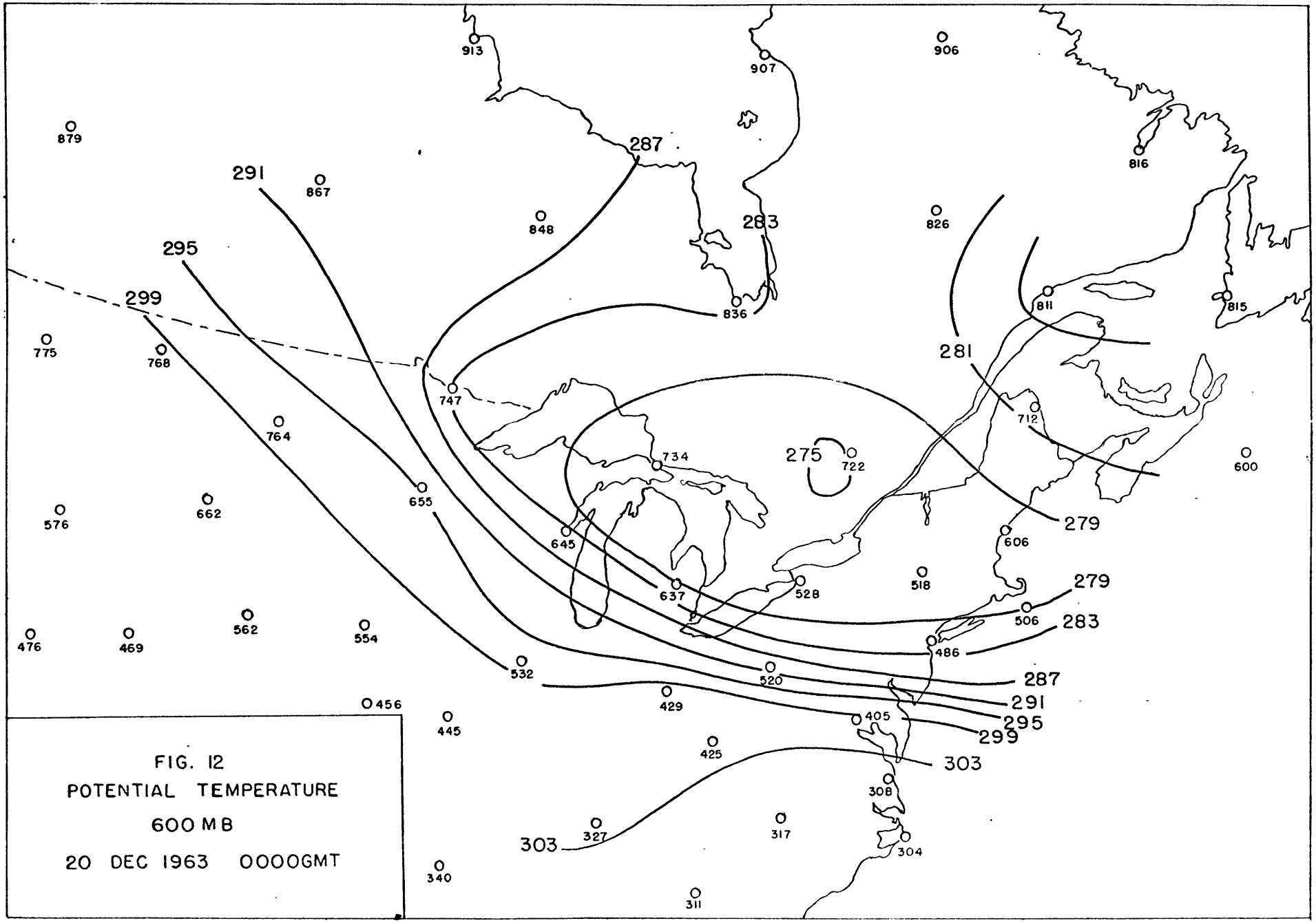

FIG. 12
POTENTIAL TEMPERATURE
600 MB
20 DEC 1963 0000GMT

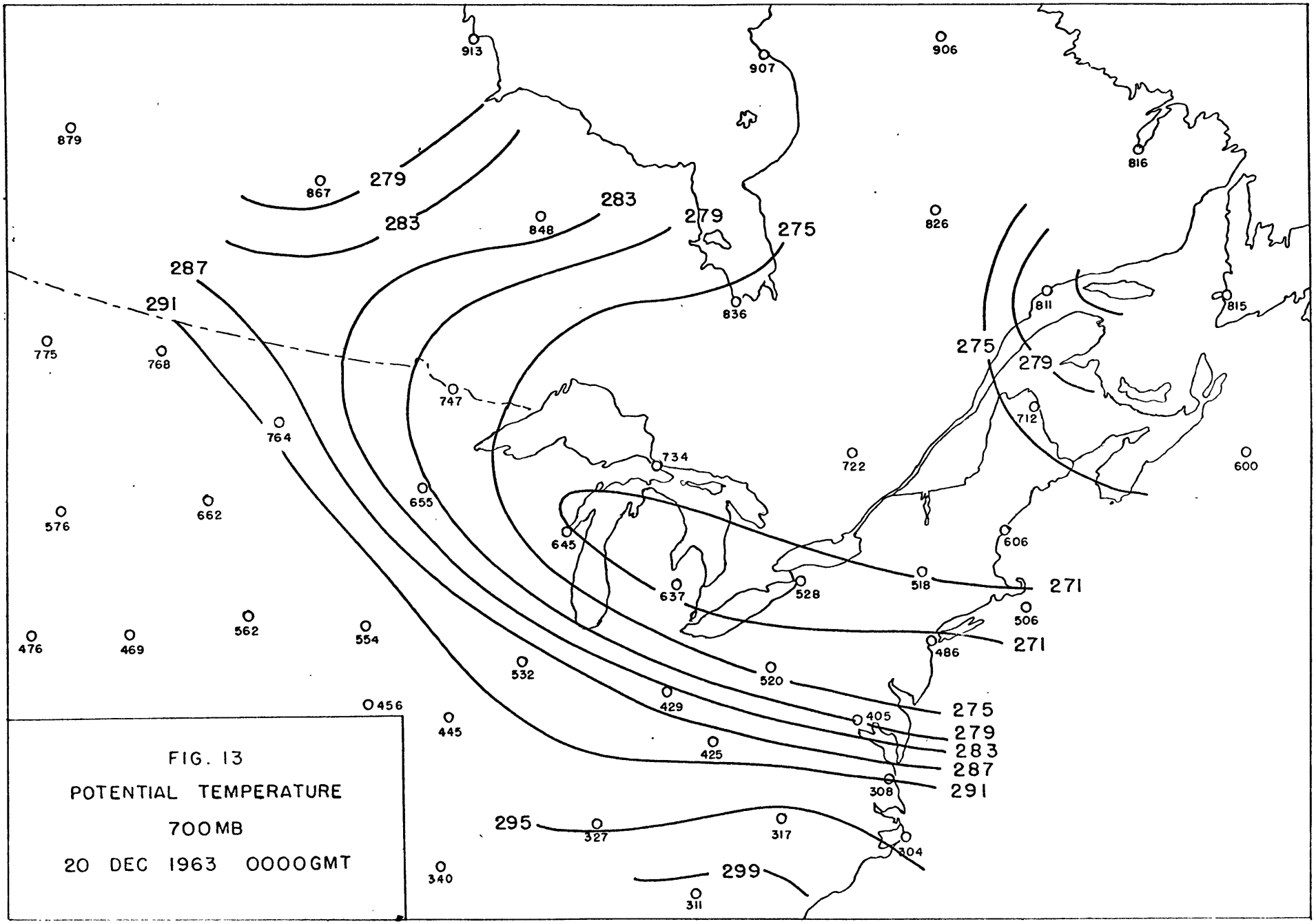

FIG. 13

POTENTIAL TEMPERATURE

700MB

20 DEC 1963 0000GMT

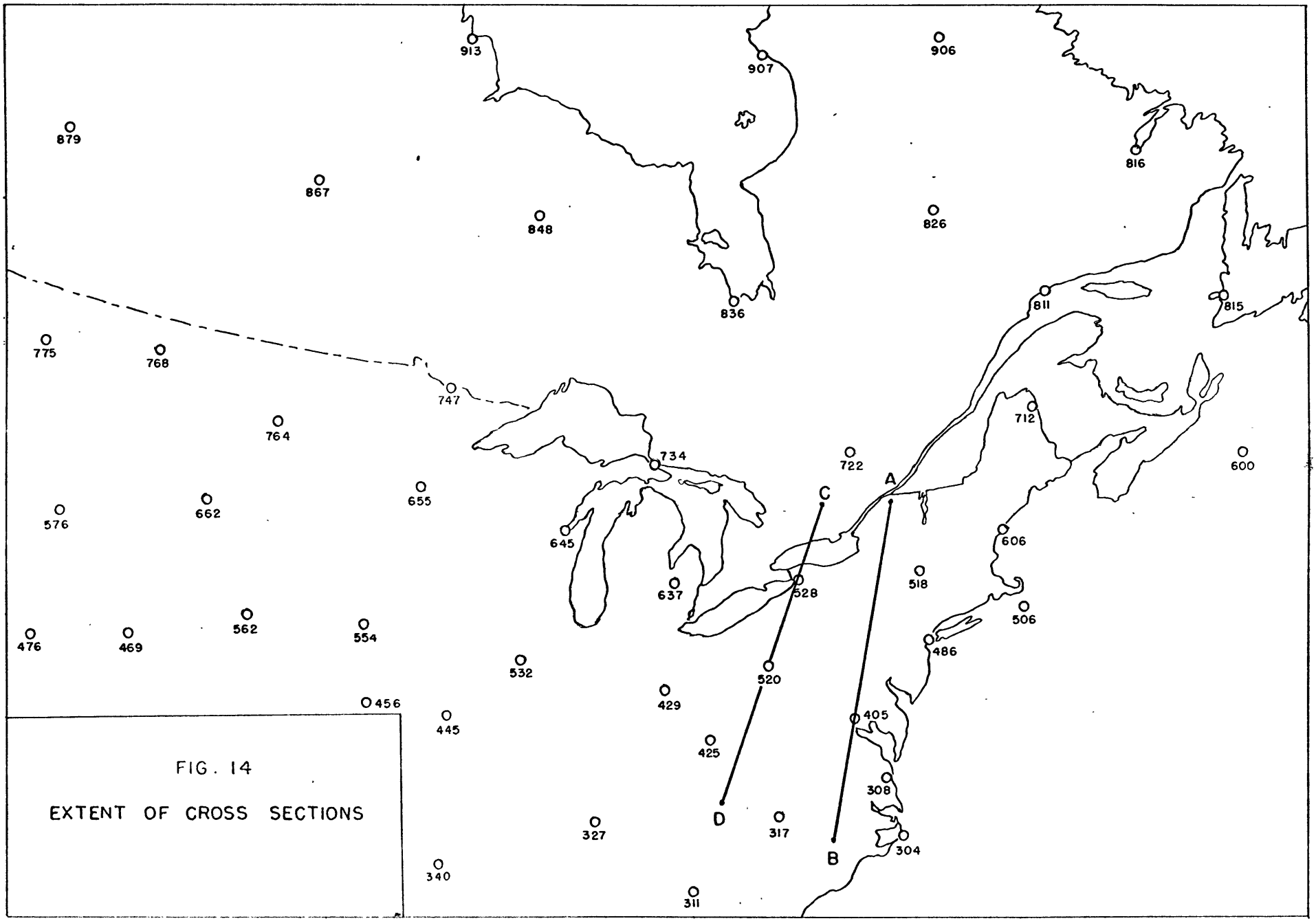

FIG. 14

EXTENT OF CROSS SECTIONS

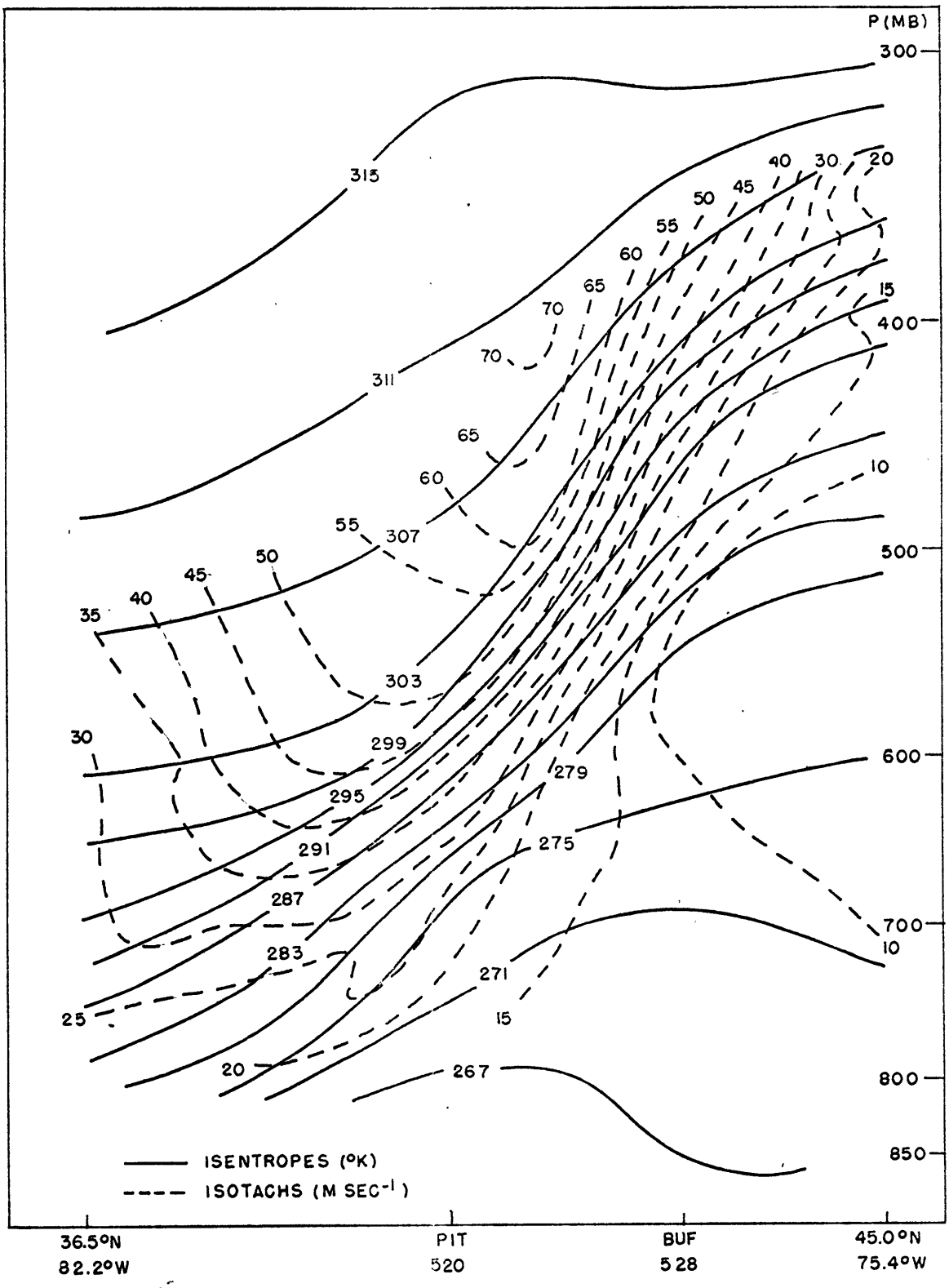

FIG. 15 20 DECEMBER 1963 0000 GMT.

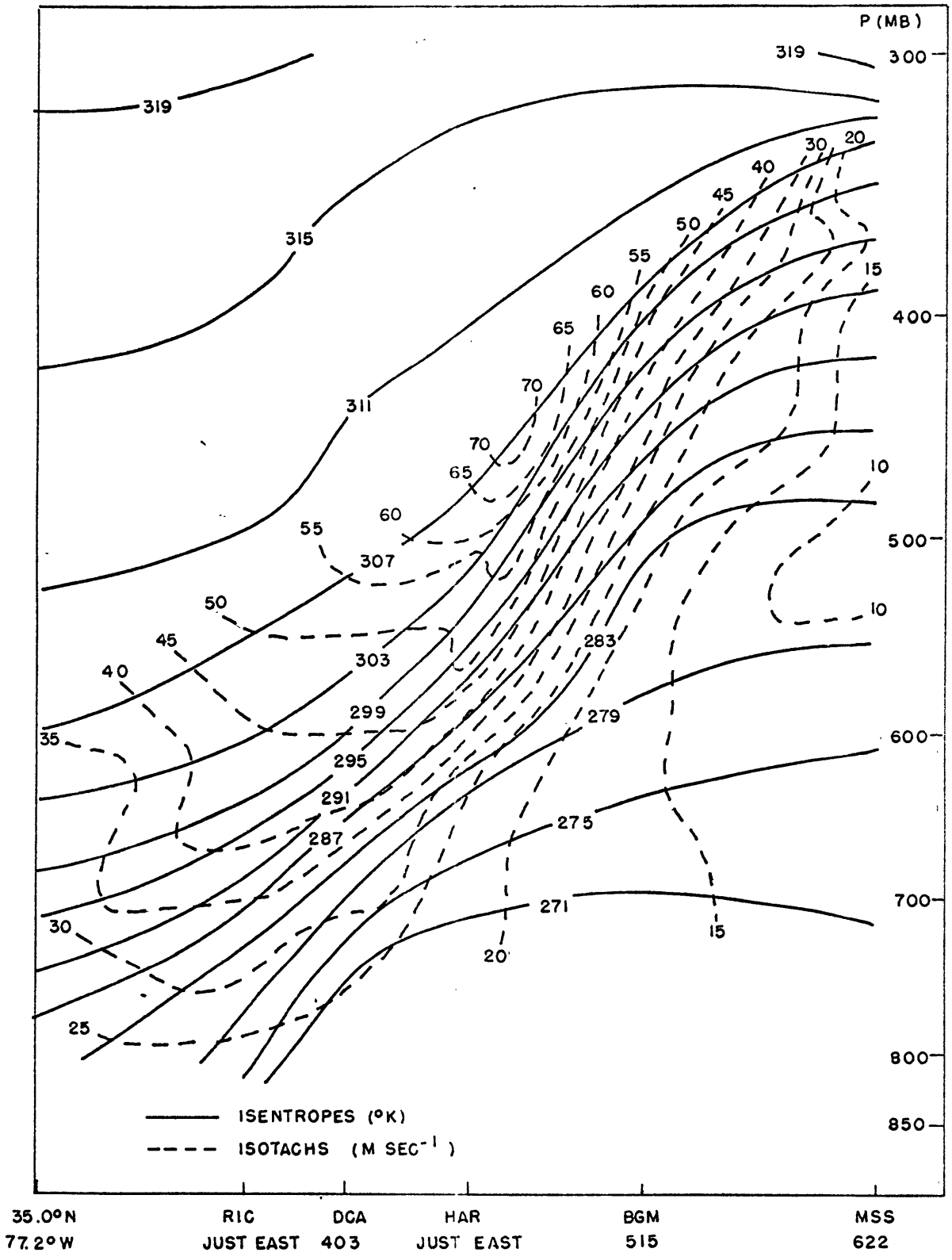

FIG. 16 20 DECEMBER 1963 0000 GMT

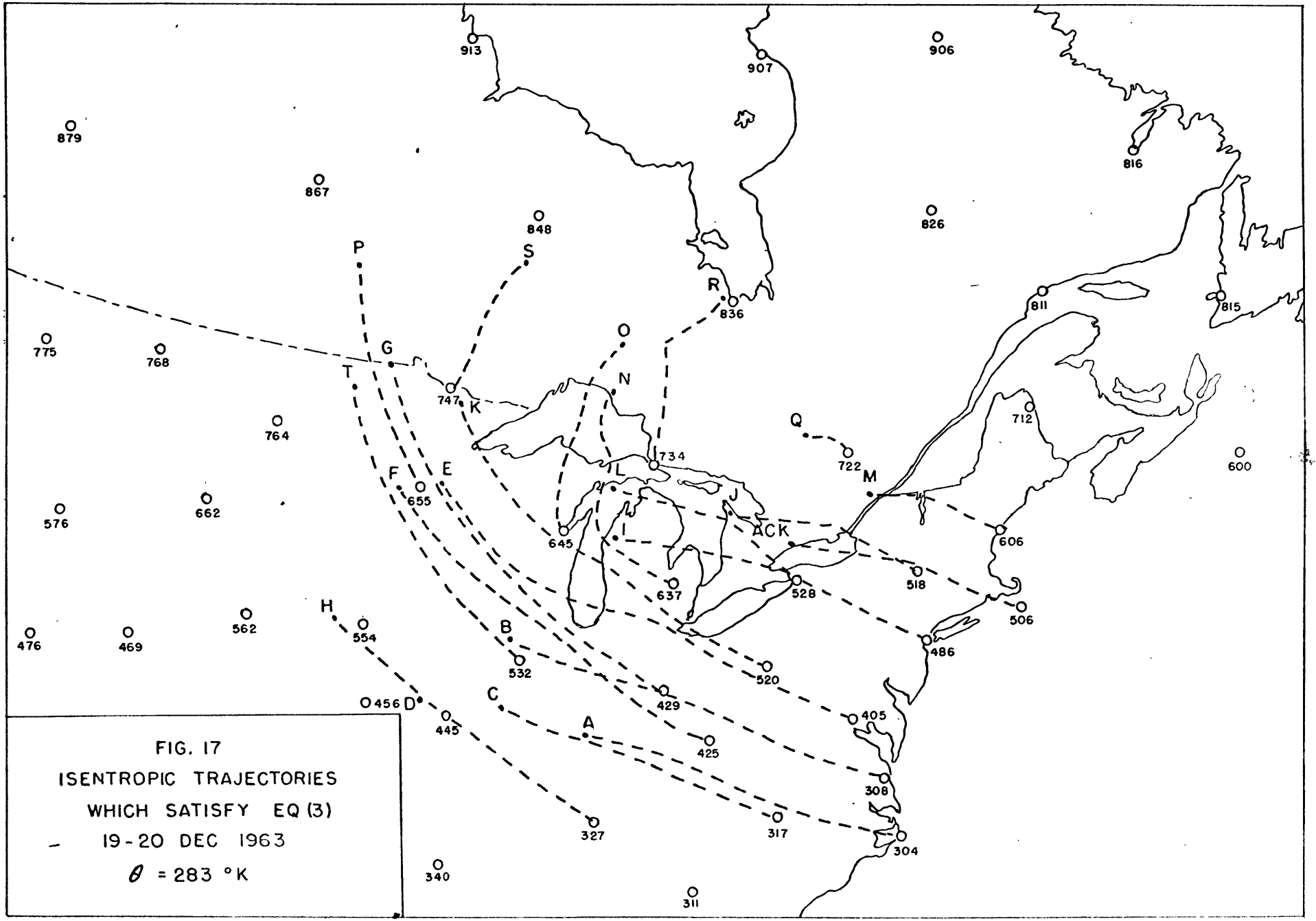

FIG. 17
ISENTROPIC TRAJECTORIES
WHICH SATISFY EQ (3)
19-20 DEC 1963
θ = 283 °K

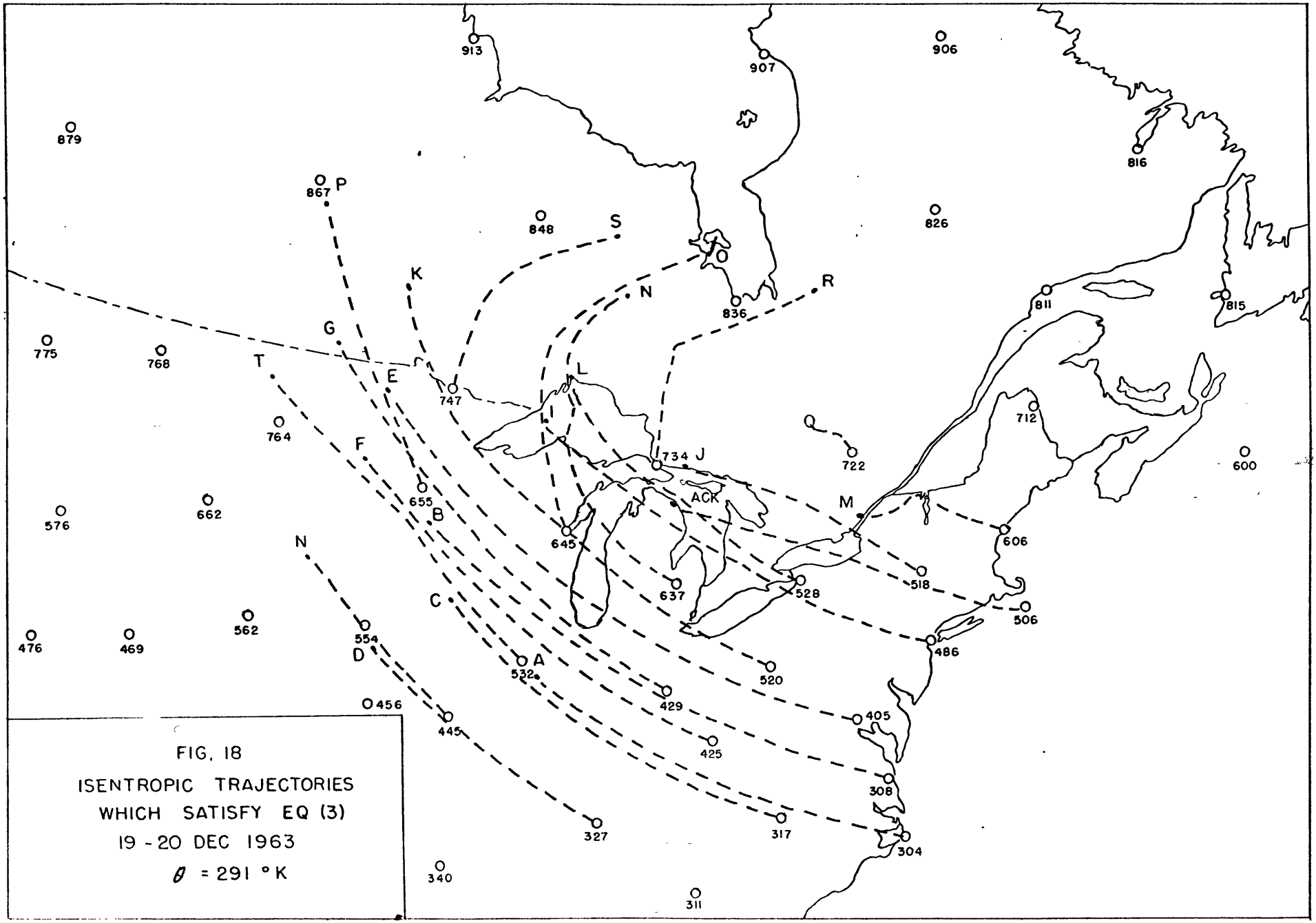

FIG. 18
ISENTROPIC TRAJECTORIES
WHICH SATISFY EQ (3)
19 - 20 DEC 1963
θ = 291 °K

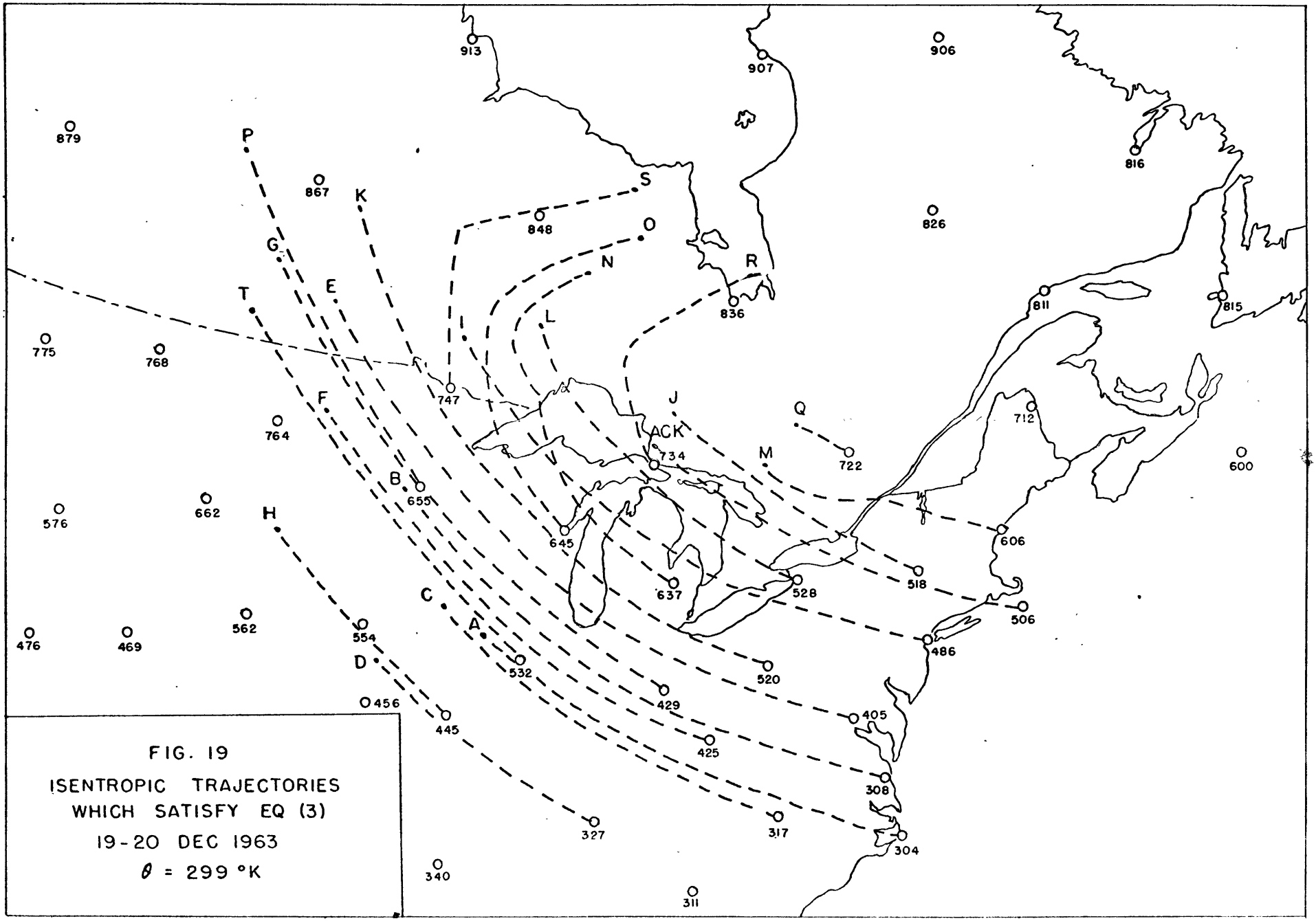

FIG. 19

ISENTROPIC TRAJECTORIES WHICH SATISFY EQ (3)

19-20 DEC 1963

θ = 299 °K

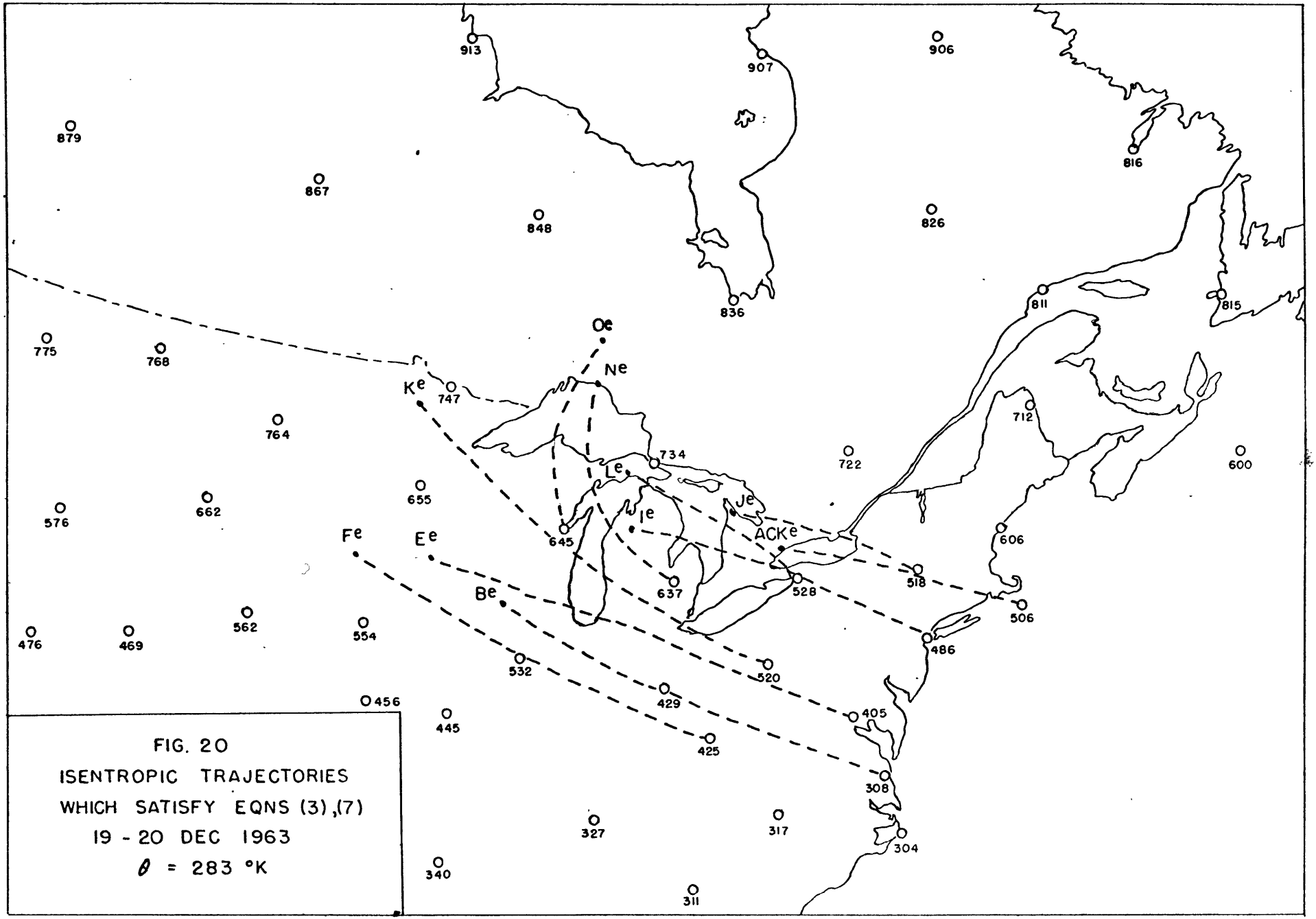

FIG. 20
ISENTROPIC TRAJECTORIES
WHICH SATISFY EQNS (3),(7)
19 - 20 DEC 1963
θ = 283 °K

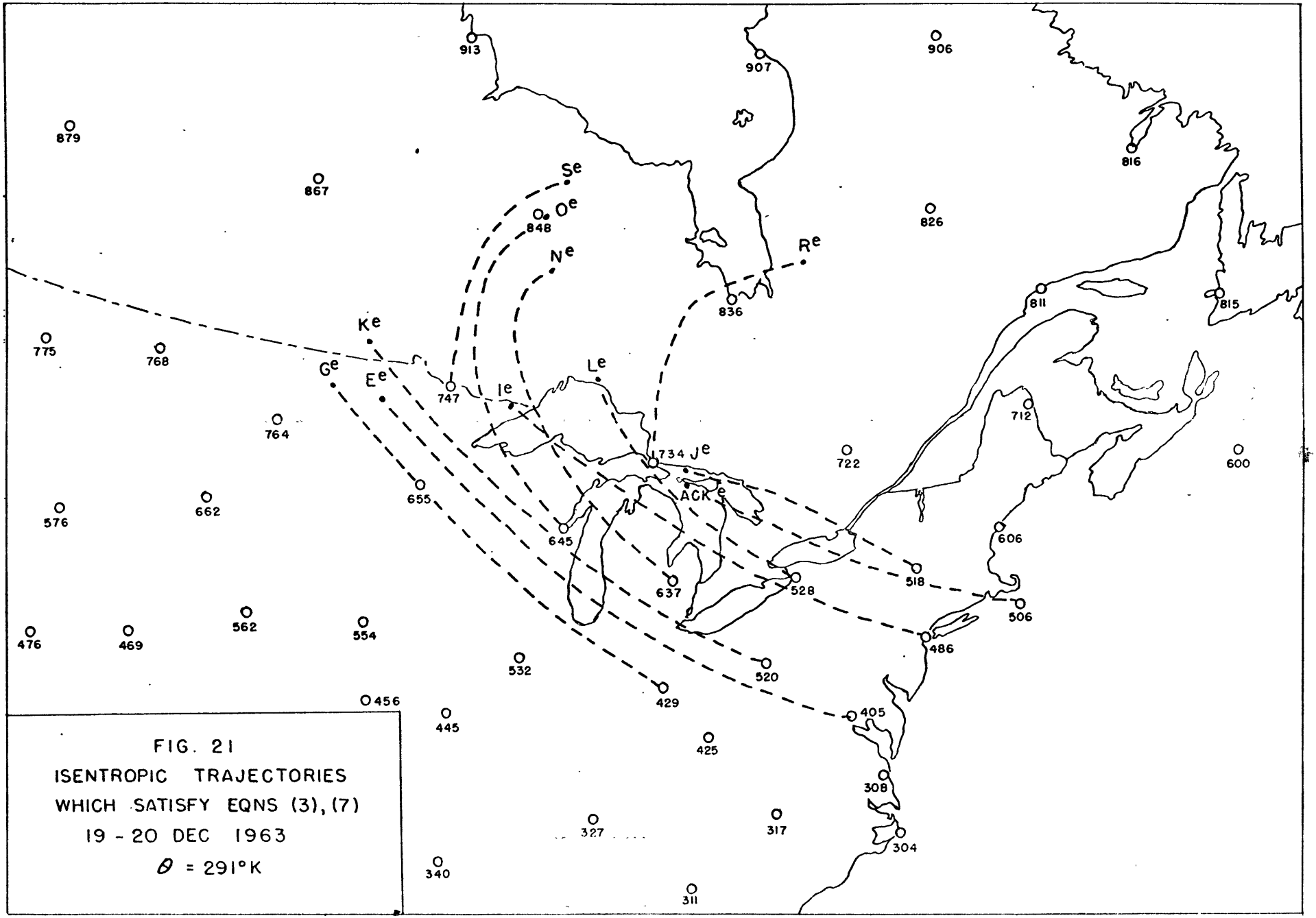

FIG. 21
ISENTROPIC TRAJECTORIES
WHICH SATISFY EQNS (3), (7)
19 - 20 DEC 1963
θ = 291°K

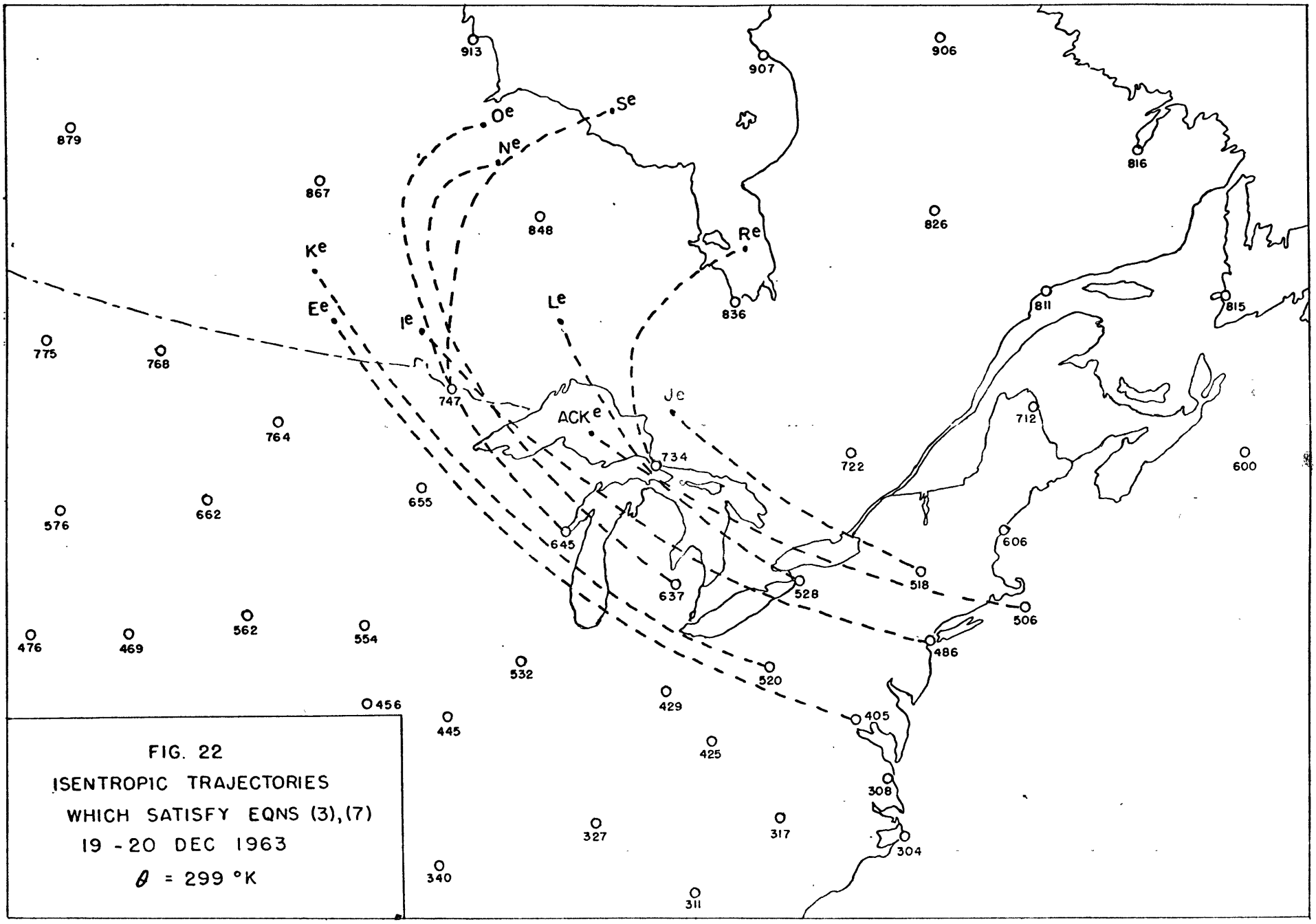

FIG. 22
ISENTROPIC TRAJECTORIES
WHICH SATISFY EQNS (3),(7)
19 - 20 DEC 1963
θ = 299 °K

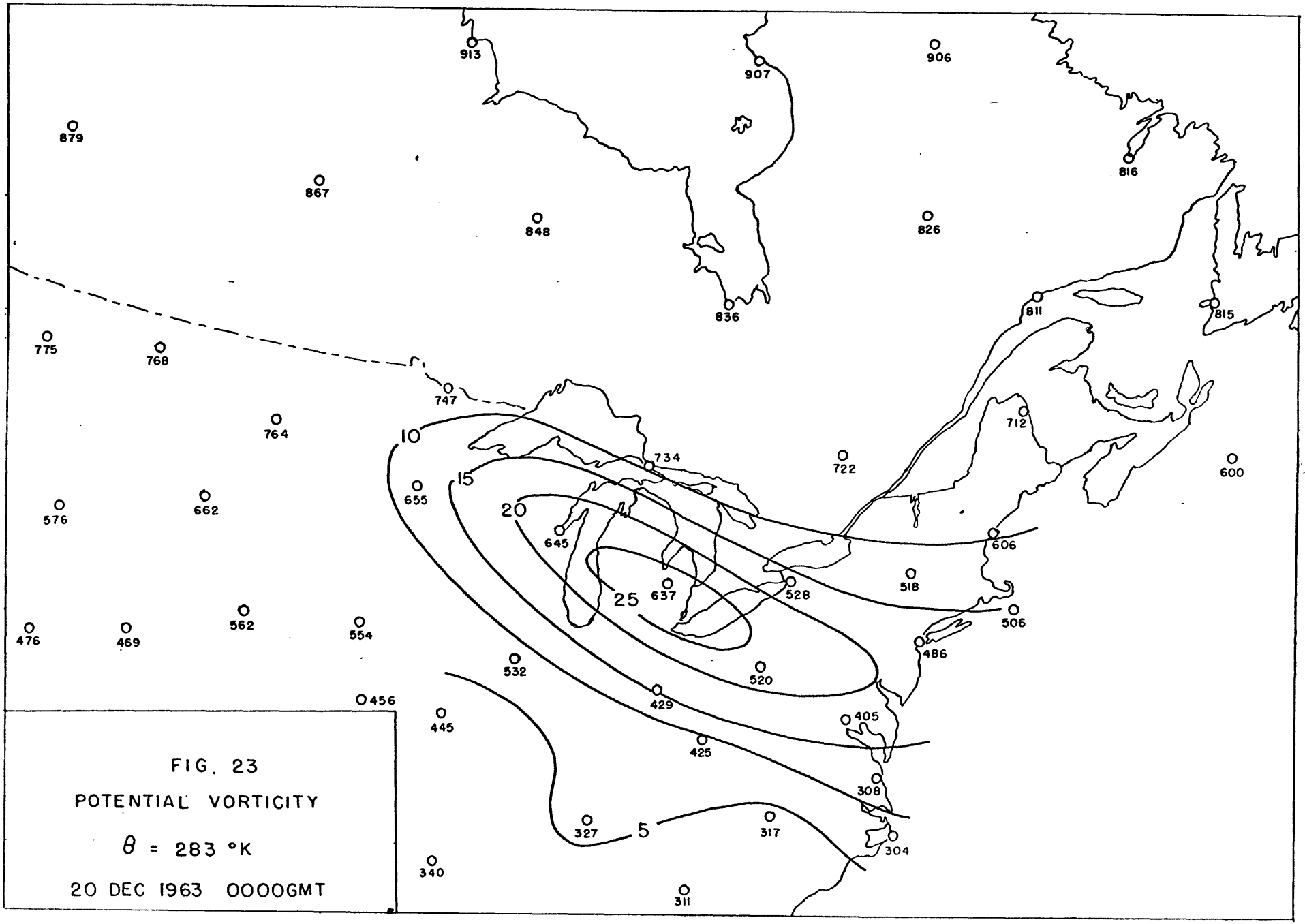

FIG. 23

POTENTIAL VORTICITY

θ = 283 °K

20 DEC 1963 0000GMT

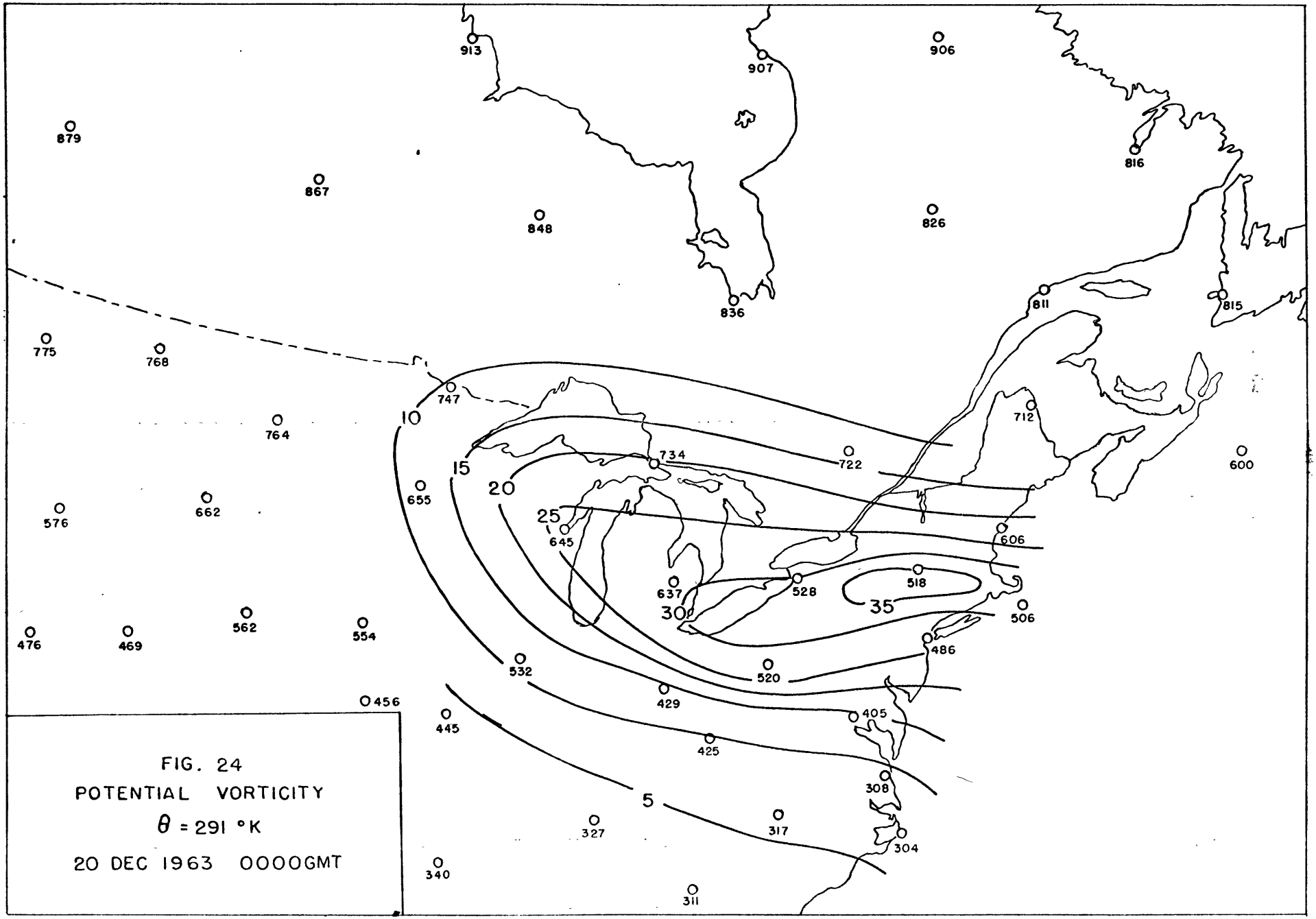

FIG. 24
POTENTIAL VORTICITY
θ = 291 °K
20 DEC 1963 0000GMT

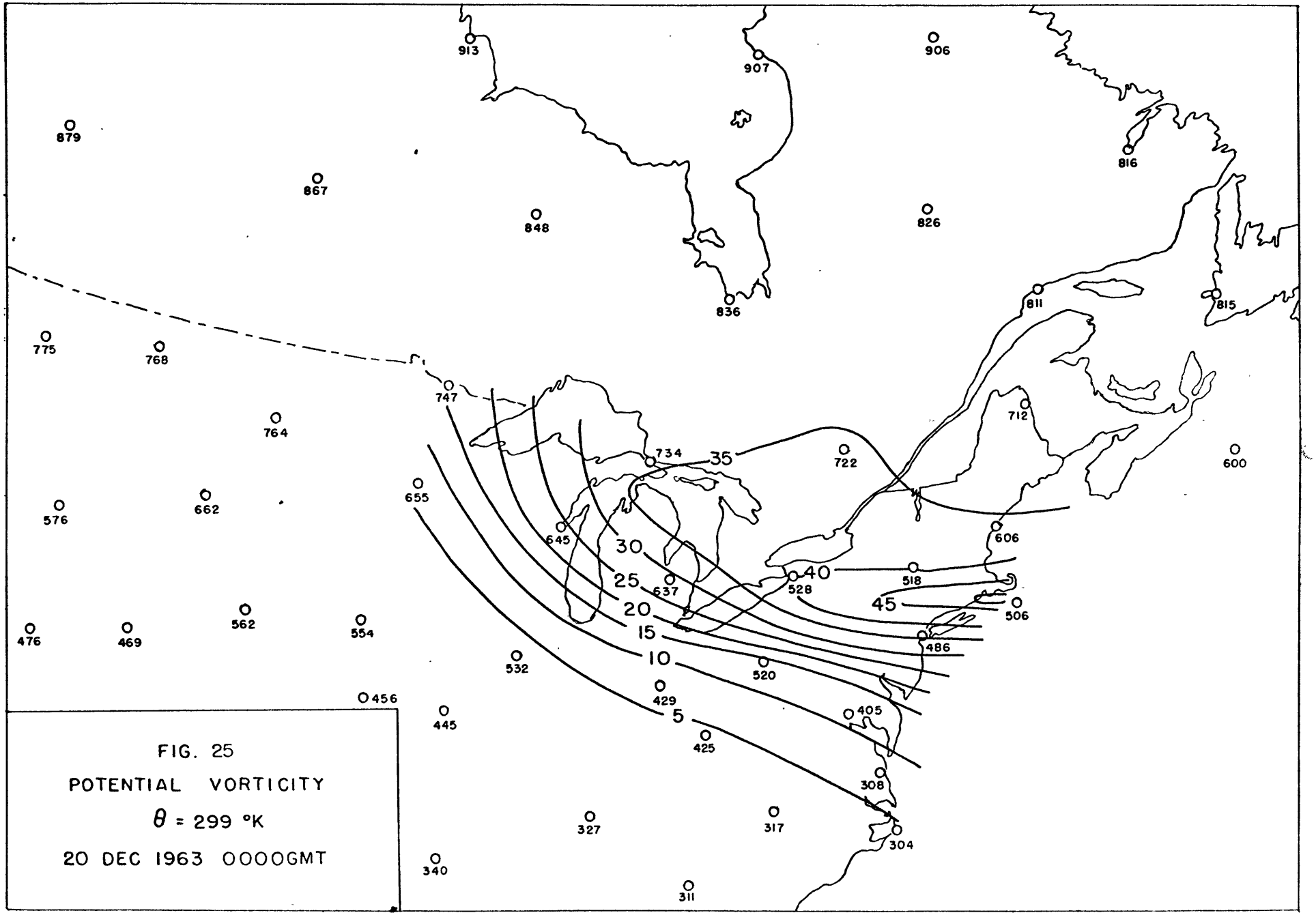

FIG. 25

POTENTIAL VORTICITY

θ = 299 °K

20 DEC 1963 0000GMT

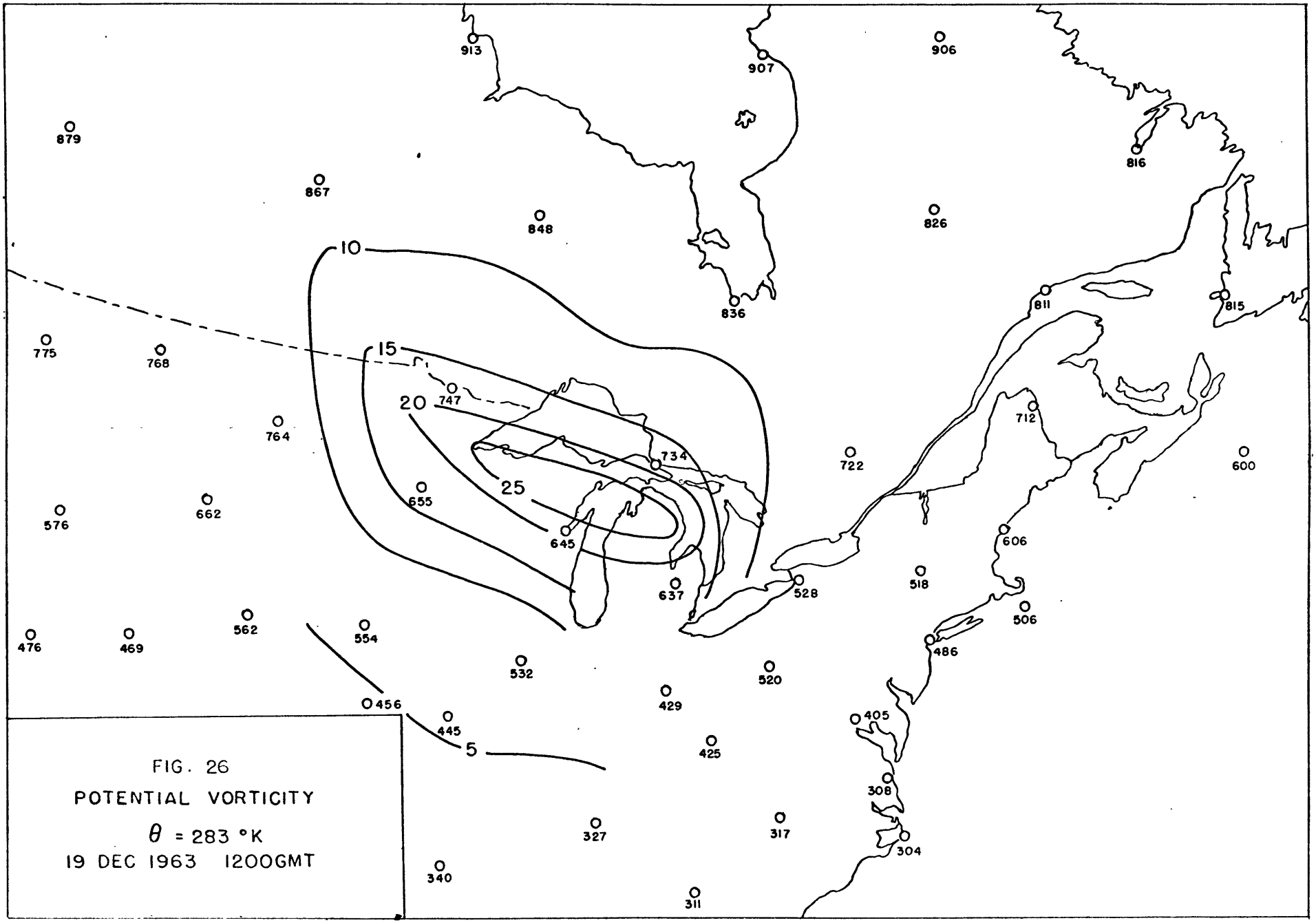

FIG. 26
POTENTIAL VORTICITY
θ = 283 °K
19 DEC 1963 1200GMT

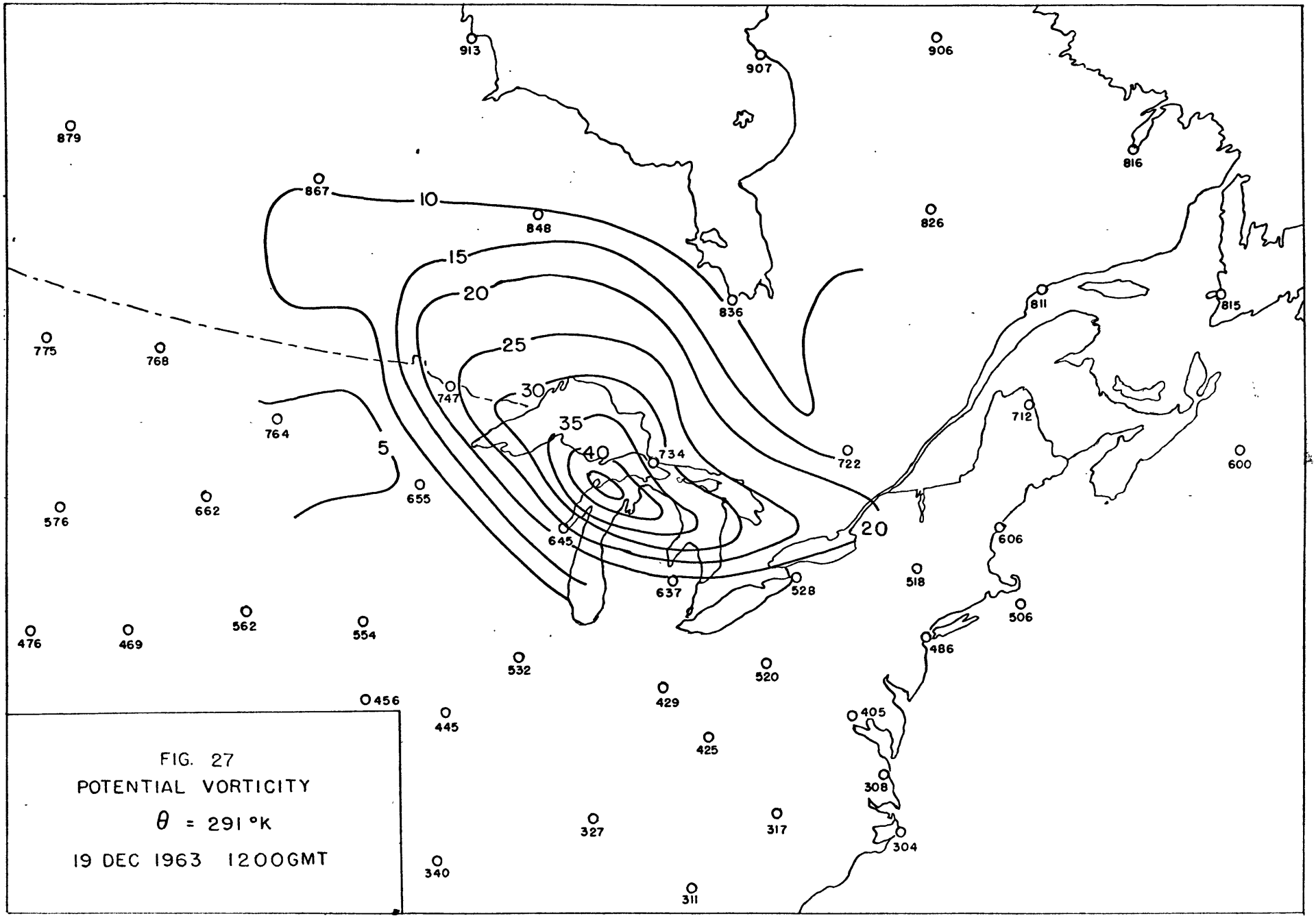

FIG. 27
POTENTIAL VORTICITY
θ = 291 °K
19 DEC 1963 1200GMT

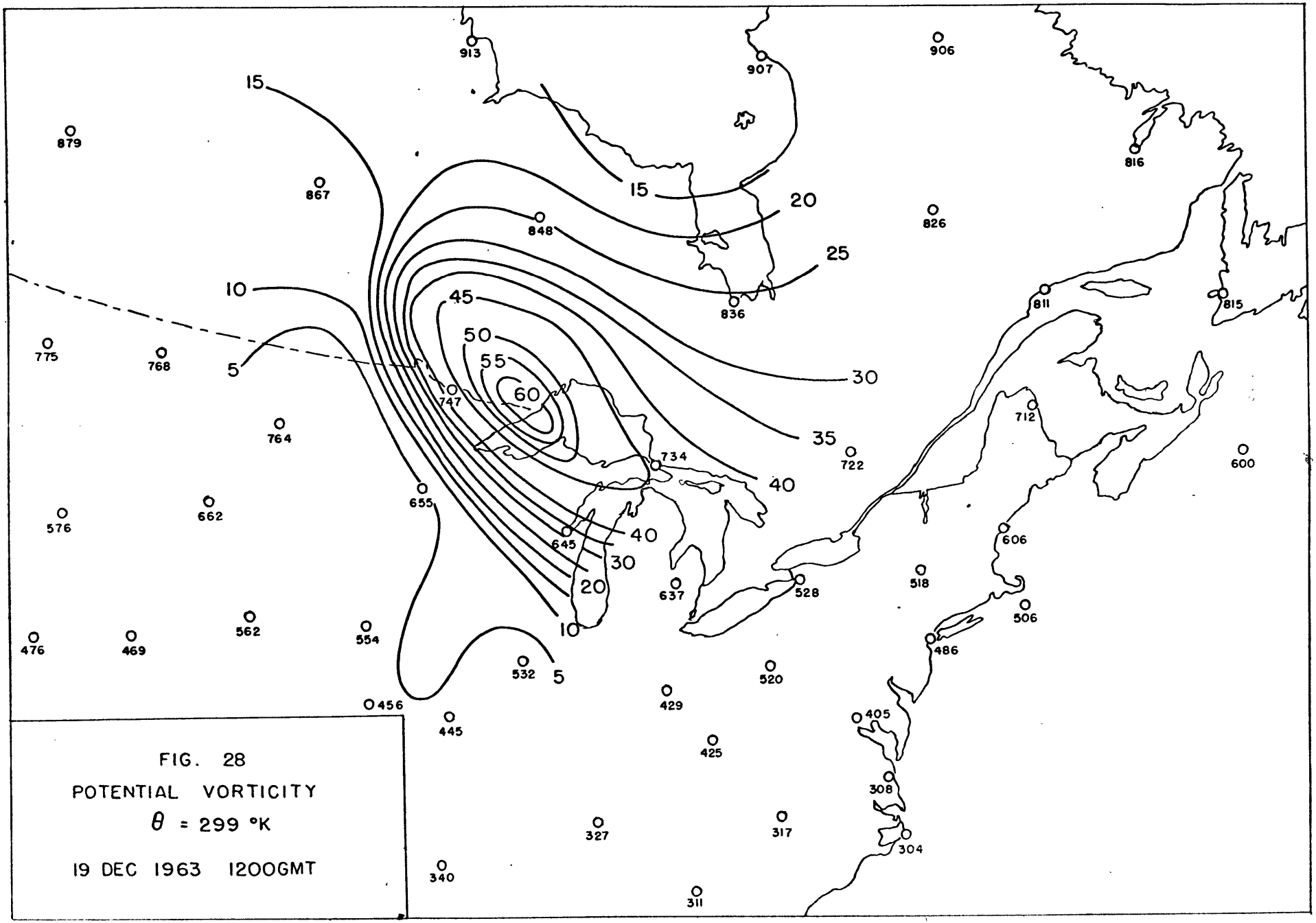

FIG. 28
POTENTIAL VORTICITY
θ = 299 °K
19 DEC 1963 1200GMT

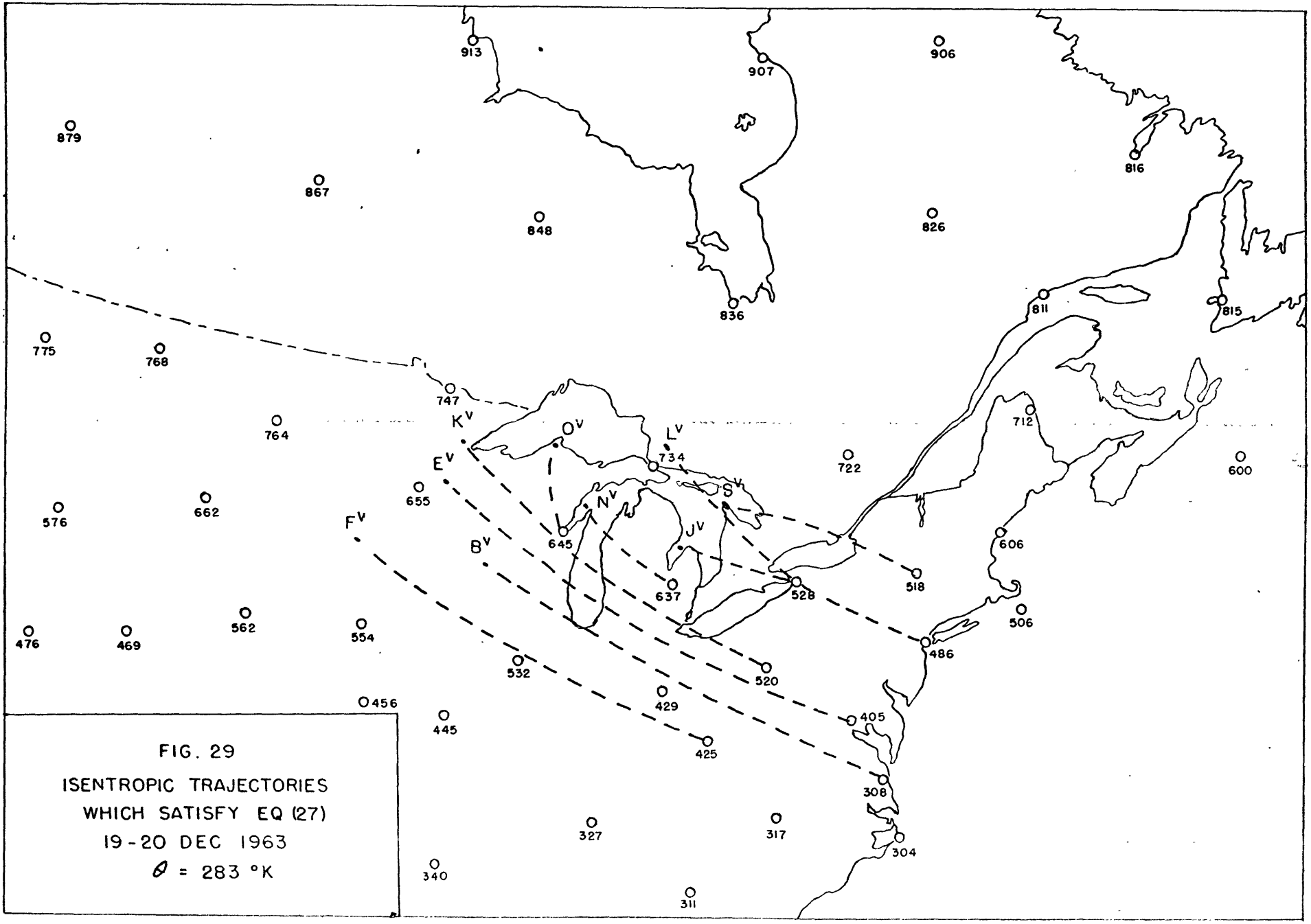

FIG. 29

ISENTROPIC TRAJECTORIES
WHICH SATISFY EQ (27)
19-20 DEC 1963
θ = 283 °K

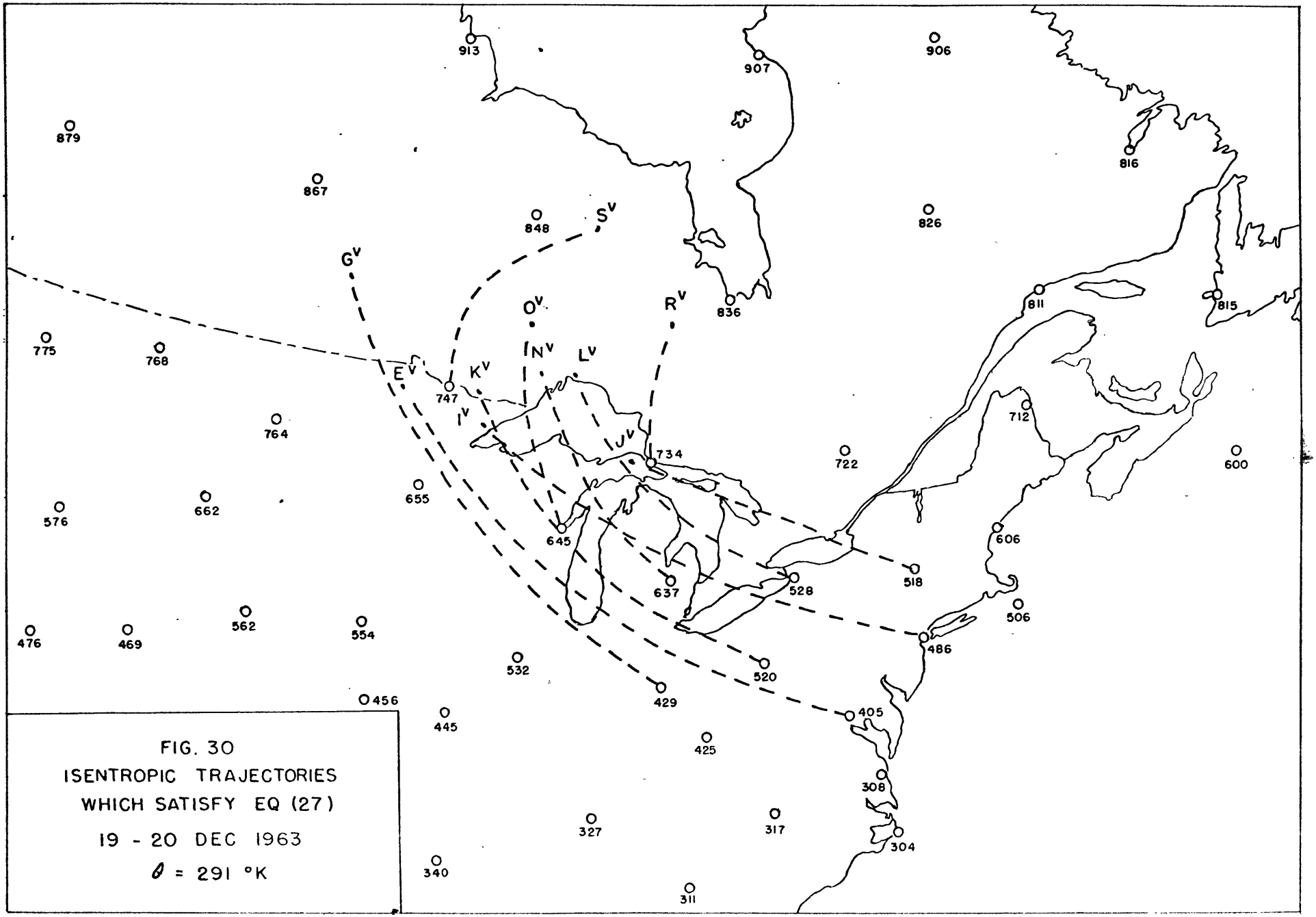

FIG. 30
ISENTROPIC TRAJECTORIES
WHICH SATISFY EQ (27)
19 - 20 DEC 1963
θ = 291 °K

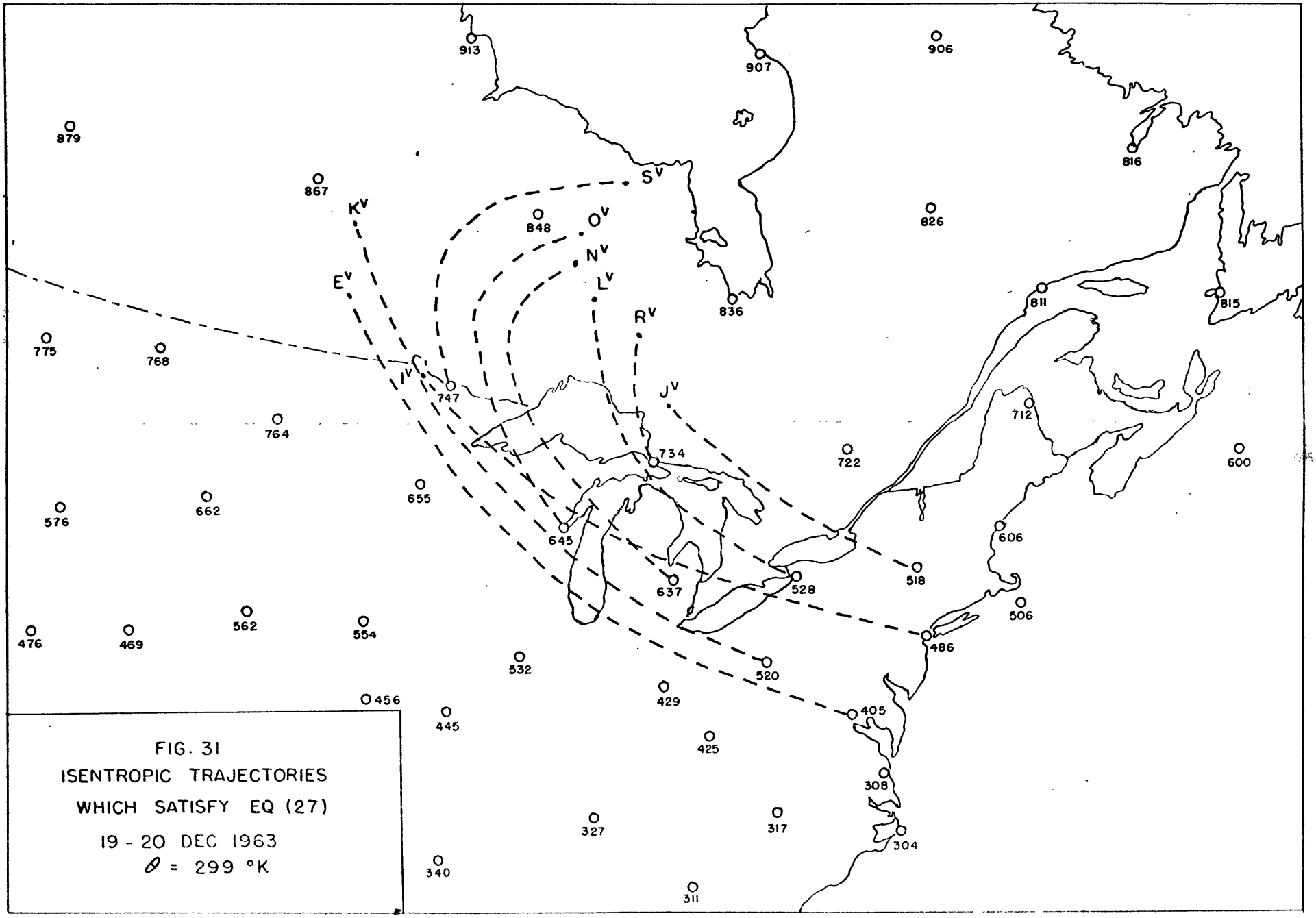

FIG. 31
ISENTROPIC TRAJECTORIES
WHICH SATISFY EQ (27)
19 - 20 DEC 1963
θ = 299 °K

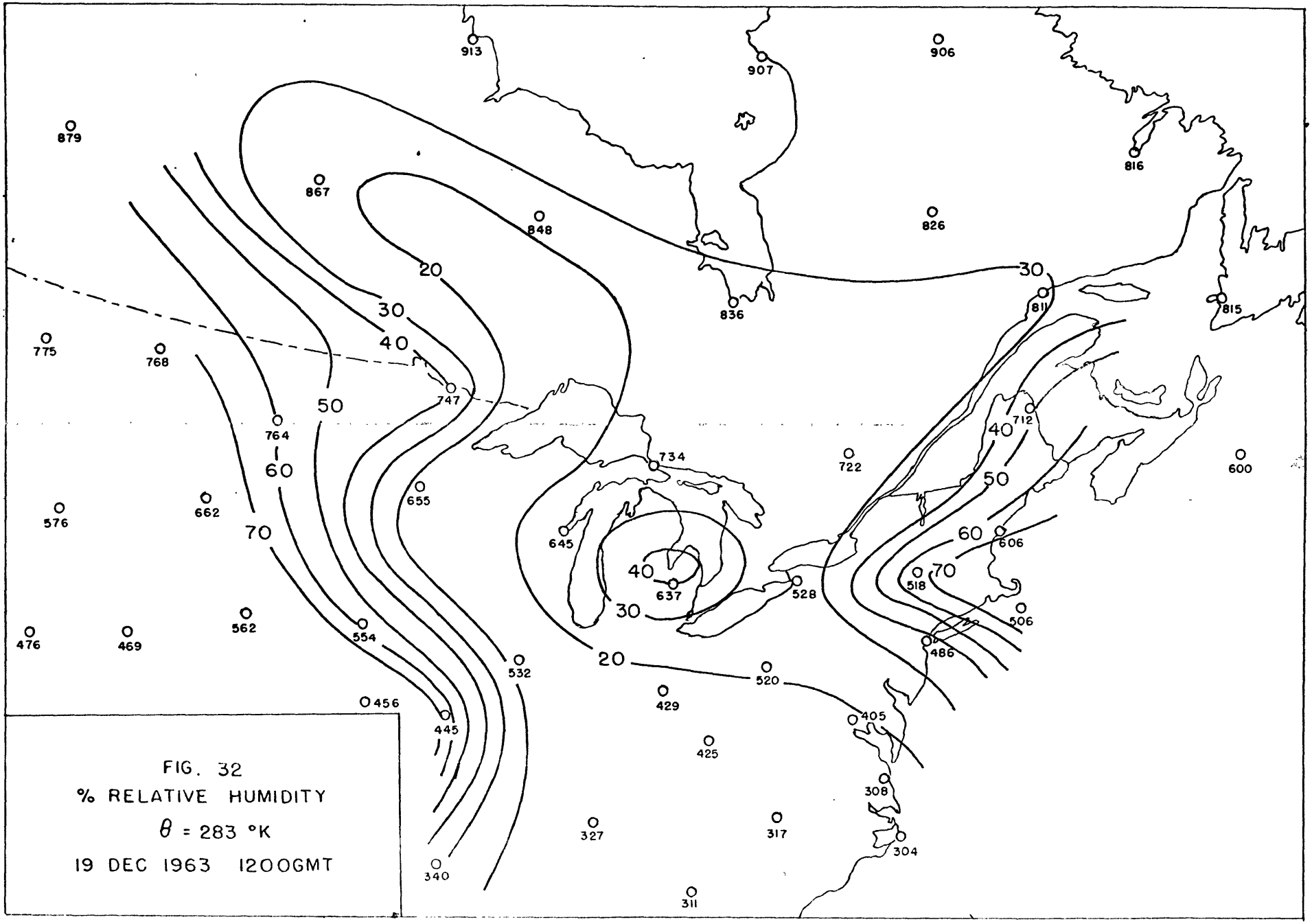

FIG. 32
% RELATIVE HUMIDITY
θ = 283 °K
19 DEC 1963 1200GMT

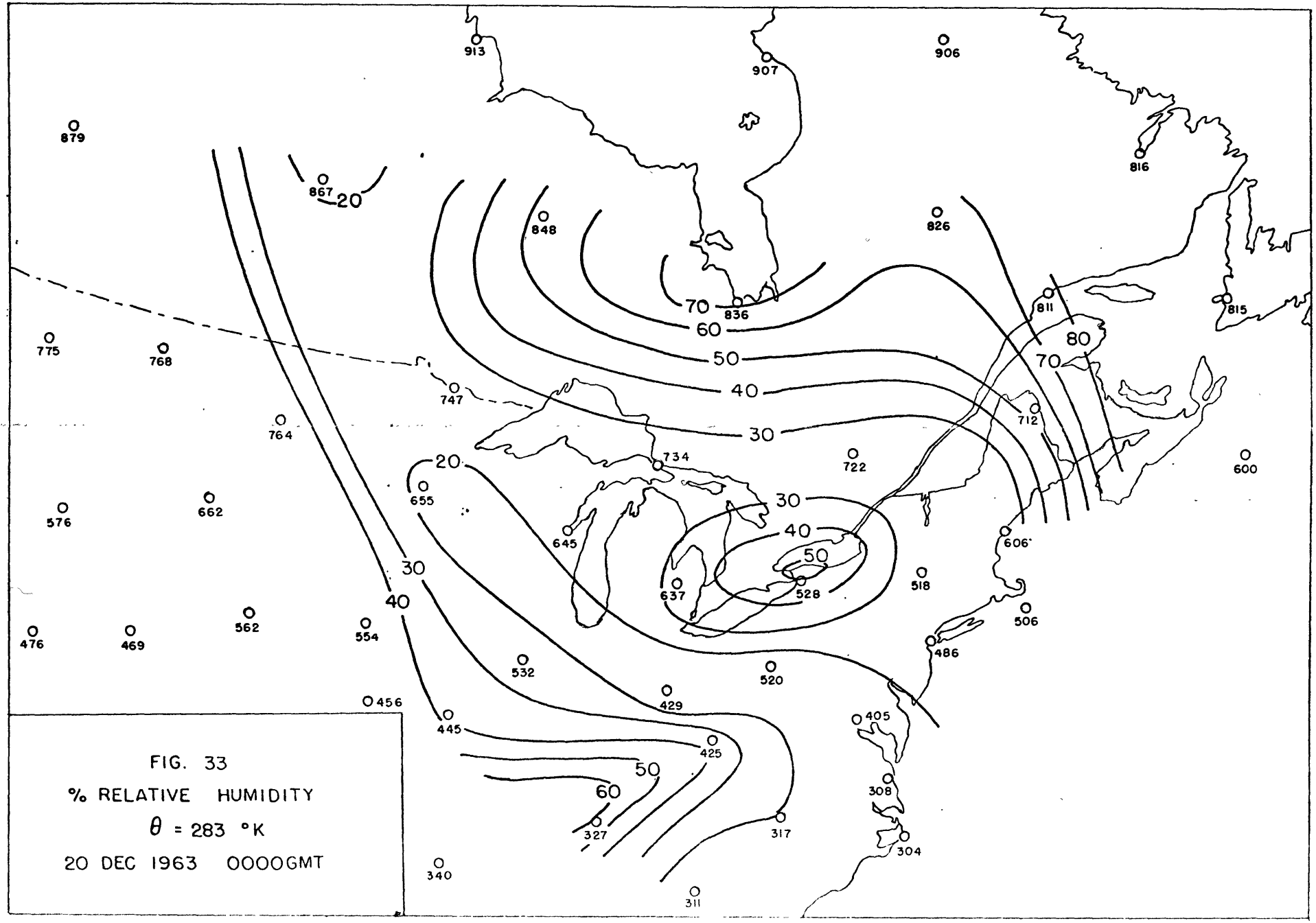

FIG. 33

% RELATIVE HUMIDITY

θ = 283 °K

20 DEC 1963 0000GMT

BIBLIOGRAPHY

Bjerknes, J., 1919: On the Structure of Moving Cyclones, Geof. Publ., 1, No. 2.

Campana, K., 1965: Frontogenetical Processes in the Upper Troposphere (unpubl. S.M. Thesis), Camb., M.I.T., 84 pp.

Charney, J., and P. Drazin, 1961: Propagation of Planetary Scale Disturbances from the Lower into the Upper Atmosphere, Jour. Geoph. Res., 66, 83-109.

Danielsen, E., 1959: The Laminar Structure of the Atmosphere and its Relation to the Concept of a Tropopause, Arch fur Met., Geophysik und Biok., A 11, 3, 293-332.

_____, 1961: Trajectories: Isobaric, Isentropic and Actual, Jour. of Met., 18, 497-486.

_____, 1964: Project Springfield Report, Defense Atomic Support Agency, 96 pp.

Djuric, D., 1961: On the Accuracy of Air Trajectories Computations, Journal of Met., 18, 597-605.

Masterson, J., et al, 1966: Strato-Mesopheric Measurements of Density, Temperature, and other Meteorological Variables in the Central Tropical Pacific, Journal of App. Met., 5, 182-188.

Moller, F., 1951: Long-Wave Radiation, Compendium of Met. (A.M.S.-Boston, Mass.) 34-48.

Reed, R., 1955: A Study of a Characteristic Type of Upper-Level Frontogenesis, Jour. of Met., 12, 226-237.

Reed, R. and E. Danielsen, 1959: Fronts in the Vicinity of the Tropopause, Arch. fur Met., Geophysik und Biok., A 11, 1, 1-17.

Reed, R., and F. Sanders, 1953: An Investigation of the Development of a Mid-Tropospheric Frontal Zone and its Associated Vorticity Field, Journal of Met., 10, 338-349.

Sanders, F., 1954: An Investigation of Atmospheric Frontal Zones (unpubl. Sc.D. Dissertation), Camb., M.I.T., 132 pp.

Staley, D., 1960: Evaluation of Potential Vorticity ..... Debris from Stratosphere to Troposphere, Journal of Met., 17, 591-622.

Staley, D., 1965: Radiative Cooling in the Vicinity of Inversions and the Tropopause, Quart. Jour. Roy. Met. Soc., 19, 282-301.

Staley, D., and Kuhn, P., 1961: Measurements of Radiative Cooling Through Two Intense Baroclinic Zones in the Middle Troposphere, Jour. of Met., 18, 208-215.

Sasaki, Y., 1962: Effects of Condensation, Evaporation and Rainfall on Development of Mesoscale Disturbances: A Numerical Experiment, Proc. Int. Symp. on Num. Wea. Pred., 477-500.